DECEMBER 2020 M.Sc. in Aircraft and Aerospace Engineering RESUL DEMİR

REPUBLIC OF TURKEY

GAZİANTEP UNIVERSITY

GRADUATE SCHOOL OF NATURAL & APPLIED SCIENCES

DESIGN AND ANALYSIS OF CONCEPT UNMANNED AERIAL VEHICLE

M.Sc. THESIS

IN

AIRCRAFT AND AEROSPACE ENGINEERING

BY

RESUL DEMİR

DECEMBER 2020

DESIGN AND ANALYSIS OF CONCEPT UNMANNED AERIAL VEHICLE

M.Sc. Thesis

in

Aircraft and Aerospace Engineering

Gaziantep University

Supervisor

Assoc. Prof. Dr. Mehmet Hanifi DOĞRU

by

Resul DEMİR

December 2020

I hereby declare that all information in this document has been obtained and presented in accordance with academic rules and ethical conduct. I also declare that, as required by these rules and conduct, I have fully cited and referenced all material and results that are not original to this work.

Resul DEMİR

ABSTRACT

DESIGN AND ANALYSIS OF CONCEPT UNMANNED AERIAL VEHICLE

DEMİR, Resul
M.Sc. in Aircraft and Aerospace Engineering
Supervisor: Assoc. Prof. Dr. M. Hanifi DOĞRU
December 2020
64 pages

This study includes the design, performance analysis, and aerodynamic improvement of a mid-range tactical UAV inspired by flying fish (Exocoetidae). By designing a dihedral wing and a curved wingtip, the static stability of the UAV was increased and vortex concentrations that cause friction were avoided. An aerodynamic body has been designed by using the narrow and long torpedo shape of flying fish. With this design approach, the reference area across the flow has been lowered and wind resistance during flight has been reduced. In this way, maximum efficiency has been achieved in performance, speed, and balance harmony. Basic requirements defined for the UAV are flight altitude over 5000 m, 12 hours endurance in the air, 100 kg payload capacity, and 150 km communication range. Computational fluid dynamics was used to construct flow models at different flow rates and angles of the aircraft and to evaluate aerodynamic coefficients. A normal aerodynamic optimization process involves the relationship between many variables. However, the aerodynamic improvement process performed in this study focused on obtaining maximum static balance at the correct wing angle. The airfoil selected for the specified purpose was kept fixed and the angle of the UAV wing with the horizontal plane was changed and compared. As a result, an unmanned aerial vehicle was designed according to the results obtained from the development process.

Key Words: Unmanned Aerial Vehicle, Concept Design, Aerodynamic Analysis

ÖZET

KONSEPT İNSANSIZ HAVA ARACI TASARIMI VE ANALİZİ

DEMİR, Resul
Yüksek Lisans Tezi, Uçak ve Uzay Mühendisliği
Danışman: Doç. Dr. M. Hanifi DOĞRU
Aralık 2020
64 sayfa

Bu çalışma, uçan balıklardan (Exocoetidae) esinlenerek tasarlanmış bir orta menzilli taktik İHA'nın tasarımını, performans analizini ve aerodinamik iyileştirmesini içermektedir. Dihedral kanat ve kıvrık kanat ucu tasarlanarak İHA'nın statik istikrarı arttırılıp, sürtünmeye neden olan vorteks konsantrasyonlarından kaçınılmıştır. Uçan balıkların dar ve uzun, bir torpido şeklinde olan yapılarına uygun aerodinamik bir gövde tasarlanmıştır. Bu tasarım yaklaşımı ile akış karşısındaki referans alan düşürülerek, uçuş sırasında rüzgar direnci azaltılmıştır. Bu sayede performans, hız ve denge uyumunda maksimum verimlilik elde edilmiştir. İHA için tanımlanan temel gereksinimler; 5000 m üzeri uçuş irtifası, 12 saat havada kalış süresi, 100 kg faydalı yük taşıma kapasitesi ve 150 km haberleşme menzili. Uçağın farklı akış hızlarında ve açılarında akış modellerini oluşturmak ve aerodinamik katsayıları değerlendirmek için hesaplamalı akışkanlar dinamiği kullanıldı. Normal bir aerodinamik optimizasyon süreci birçok değişken arasındaki ilişkiyi kapsamaktadır. Ancak bu çalışmada gerçekleştirilen aerodinamik iyileştirme işlemi doğru kanat açısında maksimum statik denge elde etmek üzerine yoğunlaşmıştır. Belirtilen amaç için seçilen kanat profili sabit tutulup, İHA kanadının yatay düzlemle yaptığı açı değiştirilerek karşılaştırılmıştır. Sonuç olarak, geliştirme sürecinden elde edilen sonuçlara göre bir insansız hava aracı tasarlanmıştır.

Anahtar Kelimeler: İnsansız Hava Aracı, Konsept Tasarım, Aerodinamik Analiz

"Dedicated to my family"

ACKNOWLEDGEMENTS

I would like to express my utmost gratitude to my supervisor Assoc. Prof. Dr. M. Hanifi DOĞRU for his guidance and encouragement during the study. I have been fortunate to have an advisor who broadens my mind and gives me the freedom space to research on my own. I owe a debt to him.

I would like to express my sincere appreciation to my cousin Medicine Doctor Dermatologist Kıvılcım Çınkır Özsaraç for her encouragement, support, and advice during the study.

Lastly, I would like to express my deepest gratitude to my family for their support and continuous encouragement in the whole stages of the study. The study would not have been completed successfully without their support and understanding.

TABLE OF CONTENTS

Page

ABSTRACT .... **v**

ÖZET .... **vi**

ACKNOWLEDGEMENTS .... **viii**

TABLE OF CONTENTS .... **ix**

LIST OF TABLES .... **xii**

LIST OF FIGURES .... **xiii**

LIST OF SYMBOLS .... **xv**

LIST OF ABBREVIATIONS .... **xix**

CHAPTER I **1**

INTRODUCTION **1**

1.1. General Introduction 1

1.2. Research Objectives and Tasks 2

1.3. Layout of Thesis 2

CHAPTER II **3**

LITERATURE SURVEY **3**

2.1. Introduction 3

2.2. Overview Of The Design Process 3

2.3. Definition of Unmanned Aerial Vehicle 5

2.4. UAVs Application Areas 6

2.5. Classification Of UAVs 6

2.6. Dihedral Wing 7

2.7. Aerodynamics of UAV 8

2.8. Aerodynamic Characteristics of Flying Fish 9

2.9. Conclusions for Literature Survey 10

CHAPTER III **11**

UAV DESIGN PRINCIPLES **11**

3.1. Introduction 11

3.2. Design Parameters ... 12
3.2.1. Mission Requirements of the UAV ... 12
3.2.2. Wing Parameters ... 13
3.2.3. Tail Parameters ... 13
3.2.4. Landing Gear Parameters ... 14
3.3. Geometric Model ... 14
3.3.1. Tail Geometry ... 16
3.4. Weight Model ... 17
3.5. Aerodynamics ... 18
3.5.1. Lift Curve Slopes ... 18
3.5.2. Maximum Lift Coefficient ... 20
3.5.3. Parasitic Drag Coefficient Estimation ... 20
3.6. Performance ... 21
3.6.1. L/D Ratio Calculation ... 22
3.6.2. Stall Velocity ... 22
3.6.3. Power Required ... 22
3.6.4. Rate of Climb ... 23
3.6.5. Time to Climb ... 23
3.6.6. Load Factor ... 23
3.6.7. Turn Performance ... 24
3.7. Mission Profile ... 25
3.7.1. Takeoff Phase ... 26
3.7.2. Climb Phase ... 27
3.7.3. Cruise Phase ... 27
3.7.4. Loiter Phase ... 27
3.7.5. Descent Phase ... 28
3.7.6. Landing Phase ... 28
CHAPTER IV ... 29
INITIAL DESIGN AND CALCULATIONS ... 29
4.1. Airfoil Selection ... 29
4.2. Calculation of Wing Loading ... 30
4.2.1. Stall Velocity Constraint ... 30
4.2.2. Cruise Speed Constraint ... 31

4.2.3. Landing Run Constraint 31
4.3. Calculation of Thrust to Weight Ratio 31
4.3.1. Takeoff Distance Constraint 31
4.3.2. Cruise Speed Constraint 31
4.3.3. Maximum Speed Constraint 31
4.4. Engine Selection 32
4.5. Propeller Sizing 33
4.6. Wing and Fuselage Design 33
4.6.1. Wing Design 33
4.6.2. Fuselage Design 34
4.6.3. Winglet Geometry Selection 34
4.7. Fuel Space Calculation 35
4.8. Landing Gear Locating and Sizing 35
4.9. Aerodynamic Analysis 37
4.9.1. Outer Geometry Calculations 37
CHAPTER V 39
COMPUTATIONAL APPROACH 39
5.1. Numerical Analysis 39
5.2. Mesh Generation 41
5.3. Numerical Method and Boundary Conditions 42
CHAPTER VI 43
RESULTS AND DISCUSSION 43
6.1. Analysis Results 43
6.2. Calculation of Aerodynamic Coefficients 49
CHAPTER VII 54
CONCLUSIONS 54
CHAPTER VIII 56
FUTURE WORKS 56
REFERENCES 59

LIST OF TABLES

Page

Table 3.1 Aircraft mission profile parameters 12

Table 3.2 Aircraft wing parameters 13

Table 3.3 Aircraft tail parameters. 14

Table 3.4 Aircraft landing gear parameters 14

Table 4.1 Similar airfoils comparison table 30

Table 4.2 Specifications of PBS TP100 turboprop engine 32

Table 4.3 Aircraft geometrical specifications 37

Table 6.1 C_L and C_D values according to wing angle for 0° AoA 49

Table 6.2 C_L/C_D ratio according to wing angle for 0° AoA 50

Table 6.3 Drag and lift force according to wing angle for 0° AoA 50

Table 6.4 C_L values according to angle of attack at each wing angle. 52

Table 6.5 C_D values according to angle of attack at each wing angle 52

Table 6.6 C_L/C_D ratio according to angle of attack at each wing angle 53

LIST OF FIGURES

Page

Figure 2.1	Aircraft design wheel	4
Figure 2.2	Three phases of aircraft design	4
Figure 2.3	Classification of UAVs applications	6
Figure 2.4	Different types of air drones	7
Figure 2.5	Lift force, drag force and angle of attack	8
Figure 2.6	Definitions of the morphometric parameters	10
Figure 3.1	Design method flow chart	11
Figure 3.2	Mission profile of the aircraft	26
Figure 3.3	TOP vs takeoff distance	26
Figure 4.1	Naca 63-412	29
Figure 4.2	Location of landing gears	36
Figure 4.3	Aircraft final geometry dimensions in mm	38
Figure 5.1	3D rendering of the UAV (front perspective)	39
Figure 5.2	3D rendering of the UAV (back perspective)	40
Figure 5.3	3D model of the wing angle at 0°	40
Figure 5.4	Mesh model of the wing angle at 0°	41
Figure 5.5	Mesh independence study results	42
Figure 6.1	Pressure (Pa) value of the wing angle at 0°	43
Figure 6.2	Velocity (m/s) value of the wing angle at 0°	44
Figure 6.3	Vorticity (1/s) value of the wing angle at 0°	44
Figure 6.4	Pressure (Pa) value of the wing angle at 5°	45
Figure 6.5	Velocity (m/s) value of the wing angle at 5°	45
Figure 6.6	Vorticity (1/s) value of the wing angle at 5°	46
Figure 6.7	Pressure (Pa) value of the wing angle at 10°	46
Figure 6.8	Velocity (m/s) value of the wing angle at 10°	47
Figure 6.9	Vorticity (1/s) value of the wing angle at 10°	47

Figure 6.10 Pressure (Pa) value of the wing angle at 15° 48
Figure 6.11 Velocity (m/s) value of the wing angle at 15° 48
Figure 6.12 Vorticity (1/s) value of the wing angle at 15° 49
Figure 6.13 Drag and lift force according to wing angle for 0° AoA 51
Figure 6.14 C_L/C_D ratio according to wing angle for 0° AoA 51
Figure 6.15 C_L/C_D ratio according to angle of attack at each wing angle 53
Figure 8.1 Foldable wing mechanism 56
Figure 8.2 Lateral movement tail mechanism 57

LIST OF SYMBOLS

α	Speed of sound (m/s)
AR_{wing}	Wing aspect ratio (-)
AR_{HT}	Horizontal tail aspect ratio (-)
AR_{VT}	Vertical tail aspect ratio (-)
b	Wing span (m)
c_{cruise}	Cruise specific fuel consumption (1/s)
c_{loiter}	Loiter specific fuel consumption (1/s)
c_r	Root chord of the wing (m)
$C_{r\,HT}$	Horizontal tail root chord (m)
$C_{r\,VT}$	Vertical tail root chord (m)
c_t	Tip chord of the wing (m)
$C_{t\,HT}$	Horizontal tail tip chord (m)
$C_{t\,VT}$	Vertical tail tip chord (m)
$C_{l\,0}$	Airfoil lift coefficient at zero angle of attack (-)
$C_{l\,design}$	Design lift coefficient (-)
$C_{L\,\alpha}$	Lift curve slope (deg^{-1})
$C_{L\,\alpha\,wing}$	Lift curve slope of the wing (deg^{-1})
$C_{L\,\alpha\,H.T}$	Lift curve slope of the horizontal tail (deg^{-1})
$C_{L\,max}$	Maximum lift coefficient of the wing (-)
$C_{m\,0}$	Airfoil moment coefficient at zero angle of attack (-)
$\overline{C_{HT}}$	Mean aerodynamic chord of the horizontal tail (m)
$\overline{C_{VT}}$	Mean aerodynamic chord of the vertical tail (m)

C_{D0}	Parasitic drag coefficient (-)
$C_{D0\,misc}$	Miscellaneous parasitic drag coefficient (-)
$C_{D0\,flap}$	Flap parasitic drag coefficient (-)
$C_{D0\,LG}$	Landing gear parasitic drag coefficient (-)
C_f	Friction coefficient (-)
D	Drag force (N)
D_H	Hydraulic diameter (m)
E	Endurance (sec)
f_{v1}	Viscous damping function (-)
F	Shape factor (-)
FF	Component form factor (-)
F_m	Force subjected to main landing gears (N)
F_n	Force subjected to front landing gear (N)
L_{HT}	Horizontal tail moment arm (m)
L_{HT}	Horizontal tail length (m)
L_{VT}	Vertical tail moment arm (m)
M	Mach number (-)
n	Load factor (-)
$n_{R\,min}$	Load factor during minimum turning radius (-)
$n_{\omega\,max}$	Load factor during maximum turning rate (-)
L_{VT}	Vertical tail length (m)
R	Turn radius (ft)
R_{min}	Minimum turn radius (ft)
Re	Reynolds number (-)
S_{wing}	Wing surface area (m^2)
S_{HT}	Surface area of the horizontal tail (m^2)
S_{VT}	Surface area of the vertical tail (m^2)
$S_{exposed}$	Exposed area (m^2)

S_{ref}	Reference area (m^2)
S_{wet}	Wetted surface area (m^2)
$S_{landing}$	Landing distance (m)
S_{α}	Obstacle clearance distance (m)
t_{cruise}	Cruising time (sec)
t_{loiter}	Loitering time (sec)
T	Air temperature (K)
T	Thrust force (N)
$T_{A\,max}$	Maximum available thrust (N)
u'	Fluctuating velocity (m/s)
v	Airspeed (m/s)
ν	Kinematic viscosity (m^2/s)
V_{cruise}	Cruise speed (m/s)
V_f	Volume of the fuel (m^3)
$W_{fuel\,burned}$	Amount of fuel burned (lbs)
V_{loiter}	Loiter speed (m/s)
V_{max}	Maximum speed (m/s)
$V_{R\,min}$	Velocity during minimum turning radius (ft/s)
V_{stall}	Stall speed (m/s)
$V_{\omega\,max}$	Velocity during maximum turning rate (ft/s)
V^*	Corner velocity (ft/s)
W	Weight (kg)
W_0	Aircraft take off gross weight (kg)
W_{empty}	Aircraft empty weight (kg)
W_{fuel}	Aircraft fuel weight (kg)
$W_{payload}$	Aircraft payload weight (kg)
ω	Turn rate (rad/s)
ω_{max}	Maximum turning rate (rad/s)

$\boldsymbol{X}$	Kinematic viscosity ratio (-)
$\bar{\boldsymbol{y}}$	Mean aerodynamic chord spanwise position (m)
$\boldsymbol{y}^{+}$	Dimensionless wall distance parameter (-)
$\boldsymbol{\Lambda}$	Wing sweep angle (°)
$\boldsymbol{\lambda}$	Wing taper ratio (-)
$\boldsymbol{\lambda_{HT}}$	Horizontal tail taper ratio (-)
$\boldsymbol{\lambda_{VT}}$	Vertical tail taper ratio (-)
$\boldsymbol{\eta}$	Propeller efficiency (-)
$\boldsymbol{\mu}$	Dynamic viscosity (kg/m.s)
$\boldsymbol{\mu_t}$	Turbulent viscosity (Pa.s)
$\boldsymbol{\phi}$	General flow variable (-)
$\boldsymbol{\rho}$	Air density (kg/m^3)
$\boldsymbol{\theta_{static\ taildown}}$	Static taildown angle (°)
$\boldsymbol{\theta_{tipback}}$	Tipback angle (°)

LIST OF ABBREVIATIONS

UAV	Unmanned Aerial Vehicle
TUAV	Tactical Unmanned Aerial Vehicle
MAV	Micro Air Vehicle
NAV	Nano Air Vehicle
MALE	Medium Altitude Long Endurance
VTOL	Vertical Take-Off Landing
HTOL	Horizontal Take-Off Landing
CFD	Computational Fluid Dynamics
CAD	Computer Aided Design
TOP	Take Off Parameter
HLG	High Lift Generating Fuselage
SST	Shear Stress Transport
RSM	Reynolds Stress Model
AOA	Angle of Attack
ROC	Rate of Climb

CHAPTER I

INTRODUCTION

1.1 General Introduction

For over a hundred years now, mankind has been designing all kinds of flying machines. These machines, which contain different ideas and features, from the prototype stage to the sky, all have a story. However, only part of it was able to achieve commercial success. People from all over the world are trying different approaches that challenge gravity. Of course, these ideas are based on science, with trial and error, have been creating designs for many years. These innovative works by new generation designers, engineers, and inventors owe everything to today's aviation era. Many people, using today's technology, produce their unique concepts. Therewithal, when experience and imagination come together, original products that can form their market are emerging.

In this field, drones are being used as unmanned aerial vehicles, with their high maneuverability and stable flight capability, being active in many areas nowadays. We can see different types of drones with different characteristics, in military, commercial, public, and private areas [1].

It is possible to see that many UAVs used or designed are similar to animals. At this point, flying animals (such as eagles, hawks, bats) were often observed when creating UAV designs. The most important factors in aviation are weight, speed, balance, and aerodynamics. The reason why these animals are preferred in the design process depends more on their aerodynamic structure. The focus of this thesis will be on designing a UAV inspired by flying fish, which are less subject to observation than the bird family in traditional unmanned aerial vehicle designs.

1.2 Research Objectives and Tasks

This study involves the design, performance analysis, and aerodynamic improvement of a mid-range UAV. In the study, a concept UAV was designed, and flow analyses were performed. The design process is based on scientific equations and experiences. A typical aerodynamic optimization process involves the relationship between many parameters, but the aerodynamic improvement process performed in this study focused on the dihedral angle the UAV wing made with the horizontal plane. These analyzes on Concept UAV were done by using Solidworks Flow Simulation software. Improvements were made on the UAV according to the data obtained.

In conclusion, according to the results of this design and improvement process in dihedral angle, maximum efficiency has been achieved in the unmanned aerial vehicle in the harmony of speed, performance, and balance.

1.3 Layout of Thesis

A literature review for aircraft designs and flying fish will be summarized in the next section and then some implications from these studies for conceptual design.

The basic parameters required for aircraft design are examined in detail in the third chapter with equations.

The fourth chapter deals with the initial design and calculations for the UAV.

In the fifth chapter, the case study is given with a computational approach.

The results obtained by flow analysis using the computational fluid dynamics tool are examined in the sixth chapter.

The interpretation of the final results is summarized in chapter seven.

The eighth chapter is about the design of some mechanisms for future works, expanding the usage area of the unmanned vehicle, and presenting a new design approach.

CHAPTER II

LITERATURE SURVEY

2.1 Introduction

In this section, studies that present different perspectives on aircraft design processes in the literature are reviewed and summarized. Besides, aerodynamic studies for Unmanned Aerial Vehicles are included. Morphometric parameters of flying fish were examined under a separate title. Information on UAV classifications and application areas has been given.

2.2 Overview Of The Design Process

First of all, before starting any design, one should have an idea of how exactly the process should begin. Each expert can state that this process should be started by considering the requirements of his/her field. For example, a designer thinks that the process starts with a new concept airplane. An engineer knows that cannot begin design without obtaining measurable data such as estimated weight, length, payload capacity [2]. When the process is looked at customer-oriented, the needs in the area where it will be used to determine the starting point of the design. All of these definitions are correct. The design is a repetitive cycle.

If it is to be defined in general terms, the aircraft design process can be expressed as aircraft sizing, basic weight improvements, analysis, preliminary design, and a more detailed optimization phase and needs determination, as shown in Figure 2.1. This process includes topics such as concept design, preliminary design, and detailed design, as shown in Figure 2.2 [3].

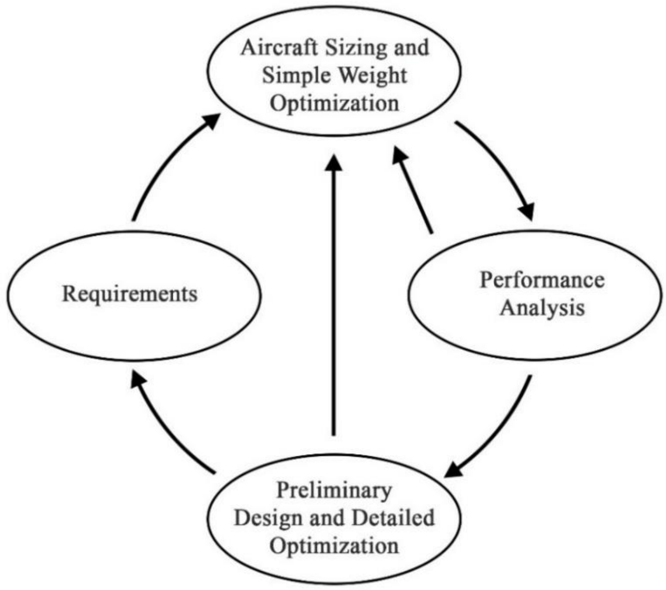

Figure 2.1 Aircraft design wheel [4].

Aircraft design is an engineering effort to build flying vehicles, taking into account the relationship between the tasks, requirements, and features defined to the aircraft. In the aircraft design process, weight, aerodynamics, aircraft structure/material, load carrying capacity for the defined mission, balance, control, propulsion systems, production, and cost are the main issues [4].

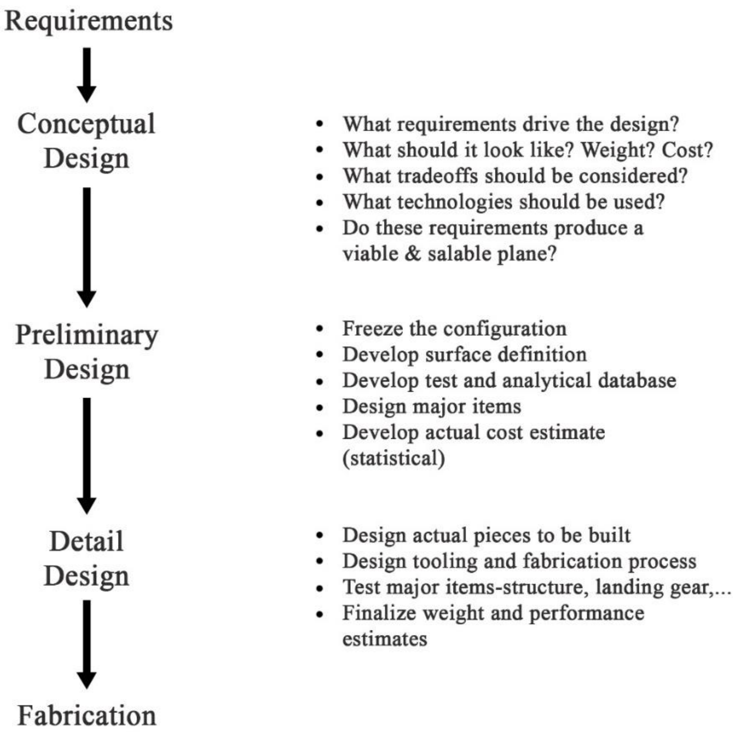

Figure 2.2 Three phases of aircraft design [3].

First, the requirements for a mission profile are determined and competitors are compared in its category. In the concept design phase, the draft of the first airframe form of the aircraft is prepared considering the needs. The preliminary design stage, which is the most important step, includes stability, structural, and aerodynamic analysis [5]. Detailed design is made after preliminary design. At this stage, the skeleton of the aircraft, other parts to be used, and surface coatings are designed. In addition to these, the production process and cost should be considered [6].

The design, performance analysis, and aerodynamic improvement of the medium-range tactical unmanned aerial vehicle were presented by Turanoğuz and Alemdaroğlu [4]. The conventional design phase is based on the employment of historical equations and experiences. Reducing engineering time and complicated algorithms for a UAV was aimed by using the aerodynamic improvement process in this study.

2.3 Definition of Unmanned Aerial Vehicle

UAV is the abbreviation of unmanned aerial vehicle, which is defined as a pilotless aircraft. We can divide it into two groups that can be controlled remotely (e.g. flown by a pilot at a ground control station) and automatically, depending on a particular flight plan. It is a widely used air vehicle for exploration, surveillance, tactical and civilian purposes [7].

Nowadays, UAVs are often used in military areas so they don't put a pilot's life at risk in combat zones. On the outside, the operation of a UAV seems simple, but it has a very complex technology in itself [8].

Nowadays, many unmanned aerial vehicles are made from lightweight composite materials to gain weight and increase maneuverability. To absorb the noise and vibrations caused by the operation of the engine of the UAV, very light composite materials are used [9]. In this way, UAVs used especially in military areas can easily fly at high altitudes. The UAVs can be equipped with many equipments according to their intended use. Among them, GPS (Global Positioning Systems), cameras, navigation systems, guided missiles, and sensors can say [10].

When the UAVs are brought together, different components are used in the construction. However, some basic components must be present in each UAV.

These; Batteries, propellers, transmitter and receiver, motors, waterproof motor frame, flight, and motor controllers [11].

2.4 UAVs Application Areas

Together with the developing technology, considering the possibilities of the UAVs, it is evident that it is already being used in many other fields with its application areas [12]. The most basic application areas are as follows. Security, inspections, surveying & mapping, search and rescue, science & research, unmanned cargo system, and aerial photography-video. In addition, the detailed classification of UAV applications is shown in Figure 2.3 [1].

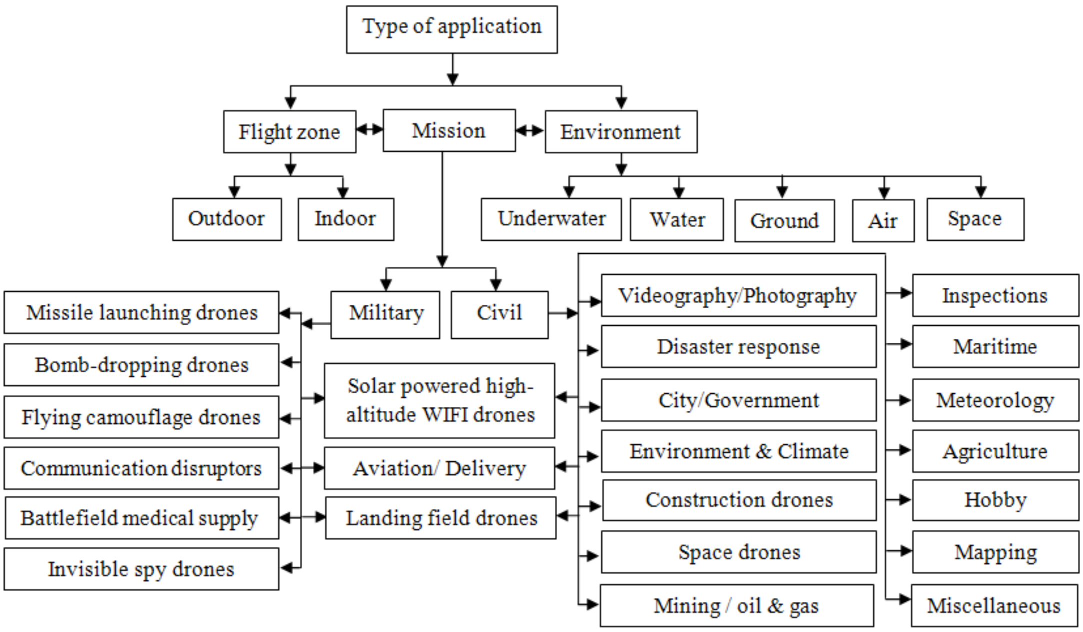

Figure 2.3 Classification of UAVs applications [13].

Today, many private companies or government agencies use UAVs in many areas such as aerospace, maritime, real estate, public services, meteorology, mining, construction and pre-works, marketing, and education [14].

2.5 Classification Of UAVs

The operational purpose of the UAVs is differentiated from other small UAV types (such as MAVs and NAVs), considering the complexity of the control system and the materials used in its manufacture. The UAVs produced according to different task requirements are classified differently according to size and configuration [15].

In this respect, it is useful to classify them. As shown in Figure 2.4, UAVs can be defined as, VTOL (vertical take-off landing), HTOL (horizontal take off landing), a hybrid model (tilt-wing, tilt-rotor, tilt-body, and ducted fan), helicopter, heliwing, and unconventional types [16].

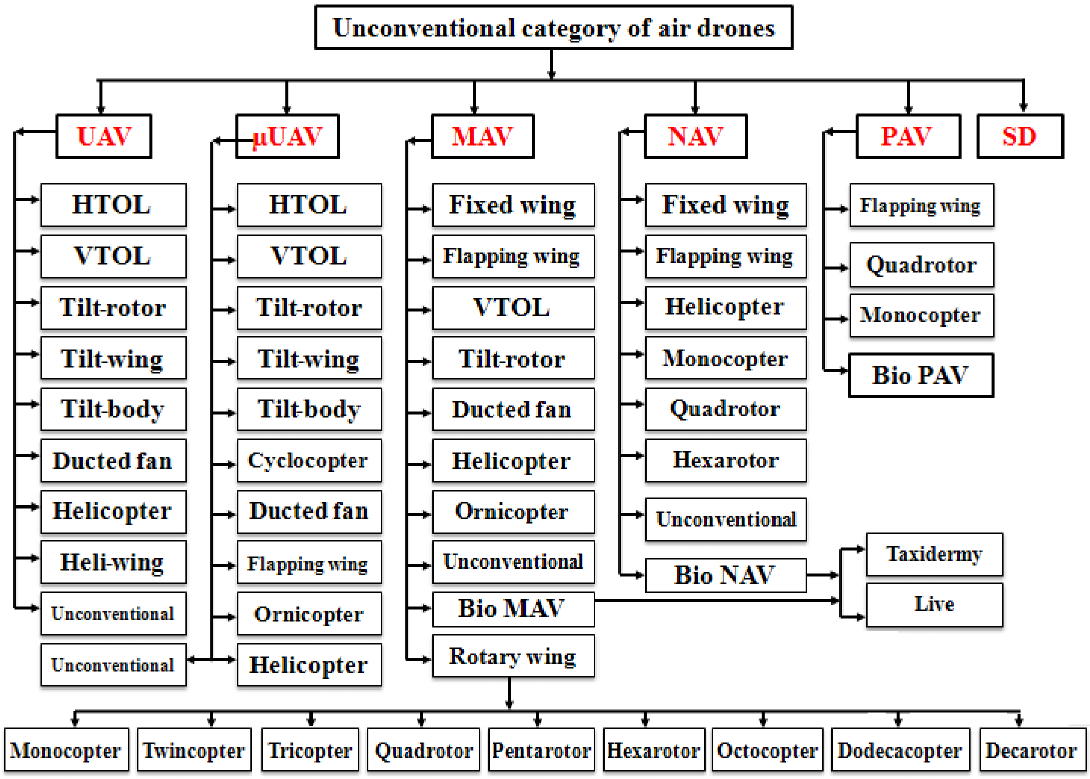

Figure 2.4 Different types of air drones [13].

Drone platforms, which have different geometries, were defined by Watts et al. They determined their advantages by addressing user demands in the field of scientific research. They have classified these platforms for their use in military, civilian, and scientific fields, taking into account drones' flight resistance, dimensions, and capabilities [17].

2.6 Dihedral Wing

In aviation, the angle between aircraft wings made with the horizontal plane is called dihedral. In gliders that can fly without a power supply, stable flight is provided by using a dihedral angle. It was discovered by George Cayley in 1809 to increase aerodynamics in aircraft [18]. The purpose of this type of wing is to give the aircraft static stability, that is, constant balance. Zero dihedral or anhedral wing is used in military combat aircraft, as it increases maneuverability. However, the use of such wings reduces the stability of the aircraft.

Wing types can be shaped differently according to different UAV types and the intended use of these UAVs, the desired performance, and parameters [19]. Many different parameters can be formed according to the location of the wing, the shape of the wing, and the angle of attachment to the body [20].

If the wing is positioned high on the UAV fuselage, it has a great effect on the dihedral. A traveling aircraft pushes air over and under the fuselage. With the wing positioned high, the air pushed by the fuselage causes the wing to lift and create more dihedral [3].

2.7 Aerodynamics of UAV

An aircraft wing in motion in the air (as shown in Figure 2.5) generates drag and lift forces [21]. Aerodynamic forces arise due to the relative motion between the airplane wing and the air. The wing profile causes pressure difference above and below the wing. Thus, a lifting force perpendicular to the flow direction occurs. Drag force occurs in the same direction as the flow direction [22]. However, another aerodynamic force acting on aircraft is the thrust. Taking the weight into consideration, flying vehicles are designed according to these forces [23].

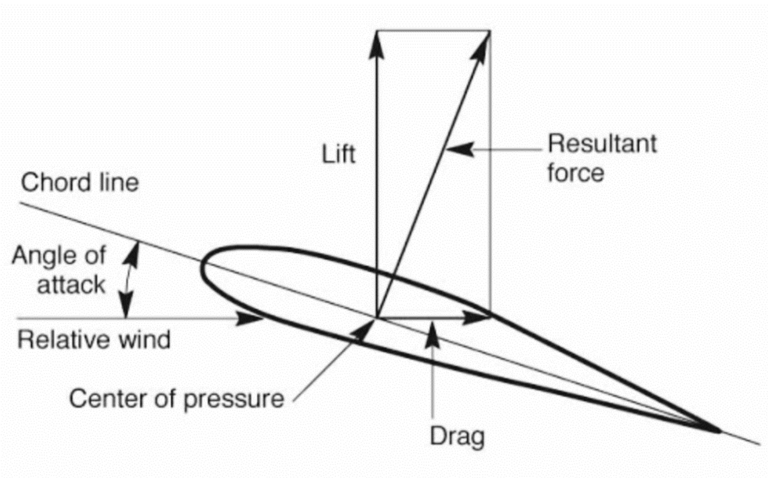

Figure 2.5 Lift force, drag force and angle of attack [23].

Using the computational fluid dynamics method in the aircraft design process, the determination of aerodynamic concepts is faster and less costly with the use of CFD tools compared to wind tunnel research [24]. As a result of the use of these tools, the performance of the designs has been increased.

Panagiotou and friends [25], presented the method of obtaining the appropriate solution for the airfoil in Medium-Altitude Long-Endurance (MALE) Unmanned Aerial Vehicles (UAV).

Bravo-Mosquera and friends [26], made an aerodynamic design of an unmanned aerial vehicle capable of surveillance to detect and transmit unusual activity in volcanoes. They calculated the aerodynamic coefficients (C_L and C_D values) for the UAV with computational fluid dynamics (CFD) simulations.

Hui When Zhao and Cees Bil [27], used computational fluid dynamics to design and aerodynamic analysis of a VTOL ducted-fan UAV at different flow rates and angles of attack. Simulated using the CFD approach to access flow patterns and calculate aerodynamic coefficients at different flight phases.

Yihua and Ziwen [28] analyzed the flow field and performance of a helicopter ducted tail rotor in hover and sideward flight using the CFD technique.

2.8 Aerodynamic Characteristics of Flying Fish

First of all, the flying fish expression is the name given to all fish belonging to the Exocoetidae family. Flying fish have an aerodynamic structure in the form of a narrow and long torpedo designed to reduce friction in water and air [29].

This allows flying fish to reach sufficient speed underwater to break the surface resistance. The most distinctive feature of these fish swimming close to the water surface is that the fins on both sides are developed. They also have bifurcated tails and pelvic fins with the lower lobe longer than the upper lobe [30]. Morphometric parameters of flying fish are shown in Figure 2.6.

As flying fishes exit the surface, they quickly move their underwater tails, pushing their bodies forward [31]. This soaring or flying process, which starts underwater, begins with a great speed, with an average speed of 60 kilometers per hour. After they climb on the surface, they start to move through the air by opening their wide wing-like fins.

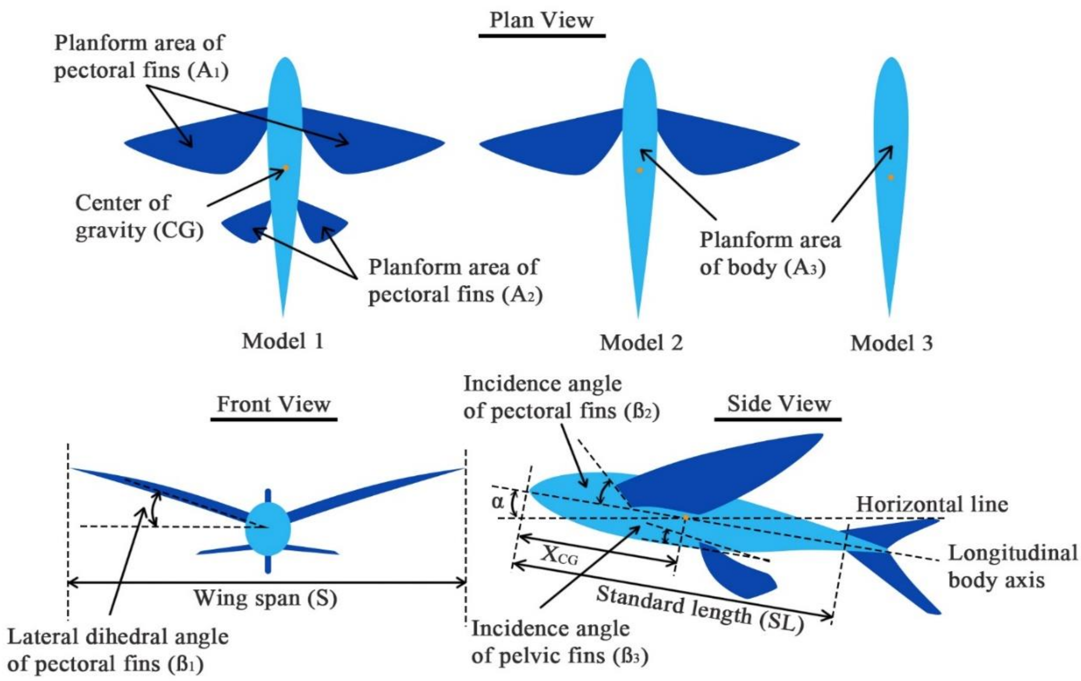

Figure 2.6 Definitions of the morphometric parameters [30].

At the point where it splashes, they can reach heights over 1.2 meters above the water surface and move 200 meters away [32]. In order to continue their gliding movements, they take off again with this thrust they create with their V-shaped tail every time they land on the water surface.

2.9 Conclusions for Literature Survey

In the literature review, the conceptual, preliminary, and detailed design stages of the UAV designs and the calculation of the need, performance, efficiency, and aerodynamic coefficients were discussed. In this section, some studies involving CFD analysis for UAVs are reviewed and different perspectives for different situations are examined to understand the approaches developed for concept UAV design.

In this thesis, a concept UAV will be designed and Solidworks Flow Simulation will be used to calculate the aerodynamic coefficients of the designed UAV at different wing angles. As a result of the aerodynamic analysis, the relationship between the angle of the wing with the horizontal plane and the drag force acting on the wing and the lift force will be examined.

CHAPTER III

UAV DESIGN PRINCIPLES

3.1 Introduction

For the tactical UAV design process, the input parameters are lift to drag ratio, range, endurance, cruise altitude, cruise speed, payload weight, and aspect ratio [33]. The cruising speed of the UAV is selected taking into account the ideal take-off gross weight. The design process is consistently advanced with an input and output analysis method [34]. The step described is a repetitive process that greatly affects the final shape of the UAV. Wing load, engine selection, landing gear selection, wing profile type, wing, and control surface geometries, thrust to weight ratio, performance parameters, and aerodynamic coefficients can be said as UAV configurations. The design process is carried out by including parameters such as communication range, endurance time, aspect ratio, cruising speed, and altitude, which are the basic requirements for the concept UAV [4].

The take-off weight of an aircraft has an effect on many parameters such as climb speed, cruising speed, maneuverability, and maximum altitude the aircraft can reach. The first performance improvement was made by optimizing cruising speed and take-off weight using conventional methods [35]. The concept design method is given as a flow chart as shown in Figure 3.1.

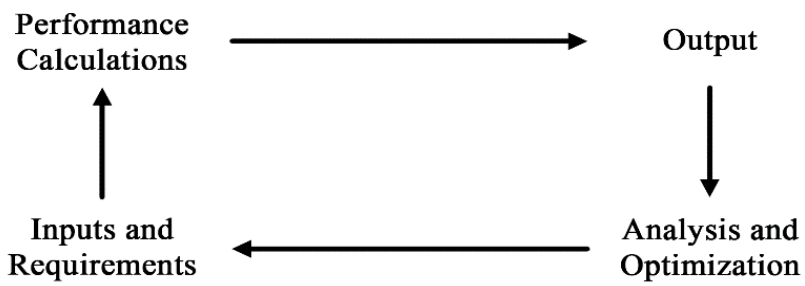

Figure 3.1 Design method flow chart [4].

3.2 Design Parameters

In order to design a stable and high performing UAV, mission parameters and design parameters such as requirements, wing configuration, wing and tail shape, and engine characteristics should be considered before making a weight estimate.

3.2.1 Mission Requirements of the UAV

Mission requirements have been selected for multi-purpose use for medium range tactical UAV design. The basic requirements defined for the design are as follows:

Endurance: 12 hours

Payload: 100 kg maximum

Cruise speed: 100 knots

Cruising altitude: 16,500 ft (above sea level)

Max. altitude: 20,000 ft (above sea level)

Table 3.1 Aircraft mission profile parameters

V_{cruise}	Cruise speed
V_{loiter}	Loiter speed
t_{cruise}	Cruising time
t_{loiter}	Loitering time
$(L/D)_{cruise}$	Cruise lift to drag ratio
$(L/D)_{loiter}$	Loiter lift to drag ratio
c_{cruise}	Cruise specific fuel consumption coefficient
c_{loiter}	Loiter specific fuel consumption coefficient

The mission profile contains many input parameters. It can be concluded that the gross take-off weight is the most important factor affecting the cruise time of the UAV compared to other parameters.

3.2.2 Wing Parameters

Along with the design of the airframe, the location where the wing is mounted on the fuselage, the aspect ratio of the wing, the taper ratio, and the chosen wing profile are important for a smooth airflow [36]. High aspect ratio is preferred in terms of wing design being more aerodynamically efficient and causing less friction. Since high wing aircraft are less subject to ground effect, the wing is positioned high in the design. However, in a high wing design, the lifting center will be higher. Thus, the center of gravity remains below the center of lift, resulting in more stability of the aircraft. In some cases, it also benefits the maximum side wind effect.

Table 3.2 Aircraft wing parameters

b	Wing span
Λ	Wing sweep
λ	Wing taper ratio
AR	Wing aspect ratio
c_t	Wing tip chord
c_r	Wing root chord
$C_{L\,\alpha}$	Lift curve slope of the aircraft
$C_{l\,0}$	Airfoil lift coefficient at zero angle of attack
$C_{m\,0}$	Airfoil moment coefficient at zero angle of attack
$C_{L\,max}$	Maximum lift coefficient of the wing
$(t/c)_{wing}$	Thickness to chord ratio of wing airfoil

3.2.3 Tail Parameters

Tail design parameters are similar to the wing. The vertical tail and the horizontal tail are lifting surfaces, as in the wing. Control surfaces separating the tail from the wing are rudder, aileron, and elevator [37]. Wing and tail are similar in terms of some design parameters such as the angle of attack, planform area, and wing profile. The most obvious difference is due to the basic function of the tail. Control, stability, and balance are the functions of the tail. The horizontal tail is used to stabilize the plane and the vertical tail to give direction [38].

Table 3.3 Aircraft tail parameters

L_{VT}	Vertical tail length
L_{HT}	Horizontal tail length
λ_{VT}	Vertical tail taper ratio
λ_{HT}	Horizontal tail taper ratio
AR_{VT}	Vertical tail aspect ratio
AR_{HT}	Horizontal tail aspect ratio
$C_{t\,VT}$	Vertical tail tip chord
$C_{t\,HT}$	Horizontal tail tip chord
$C_{r\,VT}$	Vertical tail root chord
$C_{r\,HT}$	Horizontal tail root chord

3.2.4 Landing Gear Parameters

Careful design and sizing of the landing gear are critical to the aircraft. Because the proper completion of a flight mission during the take-off and landing phase depends on the landing gear [39]. The main functions of the landing gear are to ensure the taxi to reach the required speed during take-off, to provide dynamic contact with the ground during landing, and to provide the necessary taxiing until the airplane completely loses speed. In all the cases mentioned above, the landing gear carries all the loads acting on the aircraft [40]. The aircraft has different variable speeds in all three cases. Therefore, the ground reaction causes shocks and mechanical work to occur between the landing gear. These shocks must be absorbed. For this reason, designs that can resist impacts should be provided in the aircraft structure, especially in the wing and fuselage connections [41].

Table 3.4 Aircraft landing gear parameters

F_m	Total force acting on the main landing gears
F_n	Total force acting front landing gear

3.3 Geometric Model

Wing shapes and locations have been discussed before starting the design process. Each wing model has different advantages and disadvantages. As mentioned before, wing configuration should be preferred by the intended use of the UAV. Since the main idea of this work will be a design inspired by flying fish, a high positioned wing configuration with a certain dihedral angle was preferred.

Aspect ratio and taper ratio were selected for the UAV in consideration of previous designs together with literature research [42]. Some studies reveal that AR between 8-12 performs well for more stable flight.

However, as AR increases, the wing will become heavier. Thus, the wing bending moment increases, and higher bending stress acts on the wing root. For this reason, the wing root must be designed to be durable enough to bear the weight of the wing. In addition, the AR should be kept as low as possible in this case, as increasing the weight of the wing will generate more costs [43]. With increasing AR, the maximum lift coefficient increases. In this case, the longer wing is desired. For this reason, the aspect ratio was chosen as 10.3 according to the optimum performance and cost.

When requirements such as performance, stability, and safety are required in the design, a tapered wing is desirable. The exact value of the taper ratio is achieved by detailed research and calculation on manufacturability, cost, performance, control, and stability [44]. In addition, lift distribution calculations should be made for the first estimation of the taper ratio. According to these parameters, the taper ratio of 0.43 was deemed appropriate for the wing design.

Calculation of other values is given with the following equations [45].

The wing area;

$$S_{wing} = \frac{(c_r + c_t).b}{2} \tag{3.1}$$

The wing aspect ratio;

$$AR_{wing} = \frac{b^2}{S_{wing}} \tag{3.2}$$

The taper ratio;

$$\lambda = \frac{c_t}{c_r} \tag{3.3}$$

The mean aerodynamic chord;

$$\bar{c} = \frac{2}{3} c_r \frac{1+\lambda+\lambda^2}{1+\lambda} \quad (3.4)$$

The position of average aerodynamic chord in spanwise direction;

$$\bar{y} = \frac{b}{6} \frac{1+2\lambda}{1+\lambda} \quad (3.5)$$

3.3.1 Tail Geometry

The geometric features for both tail patterns (horizontal and vertical tails) are depicted by the formulas below. Pre-sizing of horizontal and vertical tails requires knowledge of the position of the aircraft's center of gravity and the shift of the center of gravity at the desired stability level during flight. There are movable surfaces, elevator, and rudder on the tail to provide stability. However, depending on the position of the center of gravity, the weights of vertical and horizontal tails are needed [46].

The vertical tail design is very important for aircraft control and directional stability. The safety, flight characteristics, and performance of a flight are directly dependent on tail sizing. The success of the design depends on the vertical tail responsible for the control and yaw balance of the aircraft. In the preliminary design stage, an efficient vertical tail in terms of stability and control should be designed by combining the results of the experimental research and the data from theoretical assumptions [47].

The tail volume ratios;

$$C_{HT} = \frac{I_{HT} S_{HT}}{\bar{c}_w S_w} \quad (3.6)$$

$$C_{VT} = \frac{I_{VT} S_{VT}}{b_w S_w} \quad (3.7)$$

The areas of the tails;

$$S_{HT} = C_{HT} \frac{S_w}{L_{HT}} \bar{c}_w \quad (3.8)$$

$$S_{VT} = C_{VT} \frac{S_w}{L_{VT}} \bar{c}_w \quad (3.9)$$

The aspect ratios of the horizontal and vertical tail;

$$AR_{HT} = \frac{l_{HT}^2}{S_{HT}} \tag{3.10}$$

$$AR_{VT} = \frac{l_{VT}^2}{S_{VT}} \tag{3.11}$$

The mean aerodynamic chords;

$$\overline{C_{HT}} = \left(\frac{2}{3}\right) C_{HT\,root} \left(\frac{1+\lambda+\lambda^2}{1+\lambda}\right) \tag{3.12}$$

$$\overline{C_{VT}} = \left(\frac{2}{3}\right) C_{VT\,root} \left(\frac{1+\lambda+\lambda^2}{1+\lambda}\right) \tag{3.13}$$

The taper ratios of the horizontal and vertical tail;

$$\lambda_{HT} = \frac{c_{T,HT}}{c_{R,HT}} \tag{3.14}$$

$$\lambda_{VT} = \frac{c_{T,VT}}{c_{R,VT}} \tag{3.15}$$

3.4 Weight Model

There are many factors in the efficient and safe operation of aircraft in terms of weight and balance system. Incorrect weight calculation reduces the climb speed, maneuverability, and cruising speed of the aircraft.

The effects of excess weight on aircraft can be stated as follows [48]:

· The aircraft needs a high take-off speed during take-off, resulting in a prolonged take-off run.

· The maximum height limit is reduced.

· Cruising speed is reduced.

· The aircraft's cruising range becomes shorter.

· Maneuverability decreases.

· The climb angle and speed are reduced.

· The aircraft structure is overloaded, especially during the landing and take-off process.

· As the speed of the plane will be higher during the landing process, it needs a longer landing roll.

According to the studies and experiences in the preliminary design process, it starts by considering the weight effects mentioned above. At this point, weight estimation was made according to the most known and widely used method [49]. While making these predictions, some constants such as $({}^{L}/_{D})_{loiter}$ and V_{loiter} are assumed. In addition, the V_{cruise} effect and aspect ratio are taken into account. The formula is found by the sum of the aircraft's net weight, empty weight, fuel weight, payload weight, and internal component weights, as stated below.

$$W_0 = W_{empty} + W_{payload} + W_{fuel} \tag{3.16}$$

3.5 Aerodynamics

This section covers computational fluid dynamics and calculation methods of basic aerodynamic coefficients and definitions for aircraft.

$$C_L = \frac{2F_L}{\rho A V^2} \tag{3.17}$$

$$C_D = \frac{2F_D}{\rho A V^2} \tag{3.18}$$

Where C_L is the lift coefficient, C_D is the drag coefficient, F_L is the lift force, F_D is the drag force, A is the reference area, ρ is the density of the fluid, V is the flow velocity relative to the object.

3.5.1 Lift Curve Slopes

Lift curve slope is the correlation between the calculated lift coefficient for tail and wing, fuselage and angle of attack. For aircraft, the calculation of the lift curve slope should be done before the design load factor is found. Based on the calculation of the lift curve slope involves the relationship between many equations [50]. It is assumed as 2π for the thin airfoil.

$$C_{L_\alpha} = C_{L_{\alpha\,wing}} + C_{L_{\alpha\,HT}}.\eta_H.\frac{S_H}{S}\left(1-\left(\frac{d\varepsilon}{d\alpha}\right)_{downwash}\right) \quad (3.19)$$

From thin airfoil theory;

$$\frac{dC_L}{d\alpha} = 2\pi \quad (3.20)$$

The lift curve slope of the wing is calculated as follows;

$$C_{L_{\alpha\,wing}} = \frac{2.\pi.AR_{wing}}{2+\sqrt{4+\frac{AR_{wing}^2\beta^2}{\eta^2}\left(1+\frac{tan^2\Lambda_{c/2}}{\beta^2}\right)}}.\frac{S_{exposed}}{S_{ref}}.F \quad (3.21)$$

$$\beta^2 = 1 - M^2 \quad (3.22)$$

$$M = \frac{\mathrm{v}}{\alpha} \quad (3.23)$$

$$\eta = \frac{c_{l\alpha}}{2\pi/\beta} \quad (3.24)$$

$$F = 1.07\left(1+\frac{d}{b}\right)^2 \quad (3.25)$$

Where *b* is the fuselage length and *d* is the fuselage diameter.

The lift curve slope for the horizontal tail is expressed as follows [50].

$$C_{L_{\alpha\,HT}} = \frac{2.\pi.AR_{HT}}{2+\sqrt{4+\frac{AR_{wing}^2\beta^2}{\eta^2}\left(1+\frac{tan^2\Lambda_{c/2}}{\beta^2}\right)}}.\frac{S_{exposed}}{S_{ref}}.F \quad (3.26)$$

Downwash factor is calculated from the following;

$$\left(\left.\frac{d\varepsilon}{d\alpha}\right|_M\right)_{downwash} = \left.\frac{d\varepsilon}{d\alpha}\right|_{M=0}.\frac{\left.C_{L_{\alpha\,wing}}\right|_M}{\left.C_{L_{\alpha\,wing}}\right|_{M=0}} \quad (3.27)$$

$$\left.\frac{d\varepsilon}{d\alpha}\right|_{M=0} = 4.44\left[K_A K_\lambda K_H\sqrt{cos\Lambda_{\frac{c}{4}}}\right]^{1.19} \quad (3.28)$$

$$K_A = \frac{1}{AR_{wing}} - \frac{1}{1+\left(AR_{wing}\right)^{1.7}} \quad (3.29)$$

$$K_\lambda = \frac{10-3\lambda}{7} \tag{3.30}$$

$$K_H = \frac{1-\frac{h_{tail}}{b}}{\left(\frac{2l_{tail}}{b}\right)^{1/3}} \tag{3.31}$$

3.5.2 Maximum Lift Coefficient

The area of the designed wing will largely be determined by the maximum lift coefficient acting on the wing. This situation will also affect the cruise drag of the aircraft [51]. Completing such a design process should be considered as it will also affect the aircraft take-off weight.

The less reliable maximum lift measurement in design calculations is crucial in defining the aircraft's net weight. Maximum lift in high AR wings with a large wing leading edge radius and moderate sweep usually depends on the airfoil feature.

The maximum theoretical lift coefficient is given as follows [3];

$$C_{L_{max}} = (0.9)C_{l_{max}}(cos\Lambda_{c/4}) \tag{3.32}$$

3.5.3 Parasitic Drag Coefficient Estimation

Miscellaneous drag is the drag coefficient that occurs around aircraft components (such as landing gears, flaps, base area, and upswept aft fuselage) depending on the airspeed. This value is then added to the total calculated value, along with the estimated contributions for leakages and protuberances "$C_{DL\&P}$".

To find the parasitic drag coefficient, the Component Build up Method [3] is used as described below;

$$C_{D0} = \frac{\sum(C_{fc}FF_cQ_cS_{wet\,c})}{S_{ref}} + C_{D0\,misc} + C_{L\&P} \tag{3.33}$$

$$(C_{D0})_c = \frac{\sum(C_{fc}FF_cQ_cS_{wet\,c})}{S_{ref}} \tag{3.34}$$

$$C_{D0\,misc} = C_{D0\,flap} + C_{D0\,LG} \tag{3.35}$$

For turbulent flow that may occur during flight, another important factor that should not be neglected should be considered the flat plate surface friction coefficient. The term "c" in the equation refers to the expressed component.

$$C_f = \frac{0.455}{(\log_{10} R)^{2.58}(1+0.144M^2)^{0.65}} \tag{3.36}$$

The following equation is suitable for use as a component form factor for both tails and wings [3];

$$FF = \left[1 + \frac{0.6}{\left(\frac{x}{c}\right)_m}\left(\frac{t}{c}\right) + 100\left(\frac{t}{c}\right)^4\right]\left[1.34M^{0.18}(cos\Lambda_m)^{0.28}\right] \tag{3.37}$$

$$S_{wet} = S_{exposed}\left[1.977 + 0.52\left(\frac{t}{c}\right)\right] \tag{3.38}$$

FF (form factor) for both tails and wing is given in the following equation [3];

$$f = 1.07\left(1 + \frac{d}{b}\right)^2 \tag{3.39}$$

$$FF = \left(1 + \frac{60}{f^3} + \frac{f}{400}\right) \tag{3.40}$$

The parasitic drag coefficient is expressed by [3] for the landing gear as follows;

$$C_{D0\,LG} = \frac{\left(\frac{D}{q\infty}\right)}{S_{wing}} \tag{3.41}$$

The flap parasitic drag coefficient is expressed by [3] as follows;

$$\Delta C_{D0\,flap} = F_{flap}\frac{c_f}{c}\frac{S_{flapped}}{S_{ref}}\left(\delta_{flap} - 10^0\right) \tag{3.42}$$

Where δ_{flap} is in degree.

3.6 Performance

The term performance is used to describe what makes an aircraft efficient for specific purposes and its ability to accomplish a mission. The main factors that show the performance of aircraft; the rate of climb, fuel economy, stability, range, payload, take-off and landing distance, ceiling, maneuverability, and speed [52].

Factors that express the performance of the aircraft are usually due to the efficient combination and calculations between the aircraft and the powerplant. Among these factors, aerodynamic characteristics define the power and propulsion requirement for the aircraft in different flight conditions, while the powerplant refers to the power and thrust to be used. In order to achieve maximum performance, the matching of the aircraft's powerplant with its aerodynamic configurations must be in certain design conditions (such as endurance, climb, range).

3.6.1 L/D Ratio Calculation

The calculation of the theoretical L/D ratio is as follows [45];

$$\left(\frac{L}{D}\right)_{cruise} = \frac{C_L}{C_D} = \frac{C_L}{C_{D0}+KC_L^2} \tag{3.43}$$

3.6.2 Stall Velocity

In computational fluid dynamics, it is expressed as the decrease in the lift force acting on an aircraft in motion in the flow by reaching a high angle of attack. Theoretical V_{stall} has been calculated using the equation given below [45].

$$V_{stall} = \sqrt{\frac{2\left(\frac{W}{S}\right)}{\rho C_{L\,max}}} \tag{3.44}$$

3.6.3 Power Required

Since the speed of the plane is constant during the cruise, it can be written as T = D in the equation below [45].

$$T = \frac{\eta P}{V} \tag{3.45}$$

$$T = D = \frac{1}{2}\rho V^2 S C_D \tag{3.46}$$

Where η is the propeller efficiency, V is the cruise airspeed, ρ is the cruise air density and S is the wing area.

3.6.4 Rate of Climb

The maximum rate of climb is expressed as follows [45].

$$\left(\frac{R}{C}\right)_{max} = \frac{Excess\ power}{Weight} = \frac{P_{available} - P_{required}}{Weight} = \frac{(T_{A\,max} - D)V_{inf}}{W} \quad (3.47)$$

By equating the rate of climb to zero, the maximum altitude can be found. The comparison of the time needed to reach a certain altitude and the altitude obtained refers to the rate of climb. ROC is defined as the vertical component of the velocity vector of an aircraft in flight. Flying in a vertical direction provides maximum ROC performance for maximum altitude gain in a certain period of time. Thus, the acceleration of the climb causes it to travel the maximum vertical distance in a certain period of time [53].

3.6.5 Time to Climb

The area between $(R/C)^{-1}$ and the altitude gives the time to climb to reach the maximum achievable altitude.

3.6.6 Load Factor

The load factor is obtained by the ratio of the lifting force obtained from the lifting surfaces to the total weight of the aircraft. This ratio constantly changes while the aircraft is maneuvering. The load factor affecting the aircraft in straight and level flight conditions is equal to 1. As a result of wind storms or maneuvers, the load factor may be smaller or greater than one. The following equations are given for the calculation of the load factor and the maximum load factor [45].

$$n = \frac{L}{W} = \frac{1}{2}\rho V^2 C_L \frac{S}{W} \quad (3.48)$$

When $C_L = C_{L\,max}$, the maximum load factor occurs;

$$n_{max} = \frac{L}{W} = \frac{1}{2}\rho V^2 C_{L\,max} \frac{S}{W} \quad (3.49)$$

$$n = \left[\frac{\frac{1}{2}\rho V^2}{K\left(\frac{W}{S}\right)}\left[\left(\frac{T}{W}\right) - \frac{1}{2}\rho V^2 \frac{C_{D0}}{\left(\frac{W}{S}\right)}\right]\right]^{1/2} \quad (3.50)$$

3.6.7 Turn Performance

Turning performance, which is an important factor in calculating airplane performance parameters, is the aerodynamic force of the wing that causes an airplane to turn. These factors are; maximum turning rate, minimum turn radius, load factor during movement and corner speed, velocity, velocity during the maneuver, and load factor. These parameters are explained with the following equations [45].

The definition of the minimum turn radius is given as follows;

$$R_{min} = \frac{4K\left(\frac{W}{S}\right)}{g\rho\left(\frac{T}{W}\right)\sqrt{1-\frac{4KC_{D0}}{\left(\frac{T}{W}\right)^2}}} \tag{3.51}$$

Definition of velocity during the minimum turn radius;

$$V_{R_{min}} = \sqrt{\frac{4K\left(\frac{W}{S}\right)}{\rho\left(\frac{T}{W}\right)}} \tag{3.52}$$

The load factor during the minimum turn radius is as follows;

$$n_{R_{min}} = \sqrt{2 - \frac{4KC_{D0}}{\left(\frac{T}{W}\right)^2}} \tag{3.53}$$

Maximum turn rate;

$$\omega_{max} = g\sqrt{\frac{\rho}{W/S}\left[\frac{T/W}{2K} - \left(\frac{C_{D0}}{K}\right)^{1/2}\right]} \tag{3.54}$$

Definition of velocity during maximum turn rate;

$$V_{\omega_{max}} = \left[\frac{2\left(\frac{W}{S}\right)}{\rho}\right]^{1/2}\left[\frac{K}{C_{D0}}\right]^{1/4} \tag{3.55}$$

The load factor during the maximum turn rate is as follows;

$$n_{\omega_{max}} = \left(\frac{T/W}{\sqrt{KC_{D0}}} - 1\right)^{1/2} \tag{3.56}$$

Corner velocity;

$$V^* = \sqrt{\frac{2n_{max}W}{\rho C_{L\,max}S}} \tag{3.57}$$

The equations for the definition of the pull up maneuvers are as follows;

Turn radius;

$$R = \frac{V^2}{g(n-1)} \tag{3.58}$$

Turn rate;

$$\omega = \frac{g(n-1)}{V} \tag{3.59}$$

The equations for the definition of the pull down maneuvers are as follows;

Turn radius;

$$R = \frac{V^2}{g(n+1)} \tag{3.60}$$

Turn rate;

$$\omega = \frac{g(n+1)}{V} \tag{3.61}$$

3.7 Mission Profile

Mission profile refers to the stages in which different environments and events occur for an aircraft. It is also defined as the scenario required to determine the design parameters of the aircraft. Each aircraft type has a specific mission profile. The mission profile is given in Figure 3.2 as take-off, climb, cruise, loiter, descend, and landing, respectively [54]. The first weight estimation is expressed below with the mission profile and Raymer method.

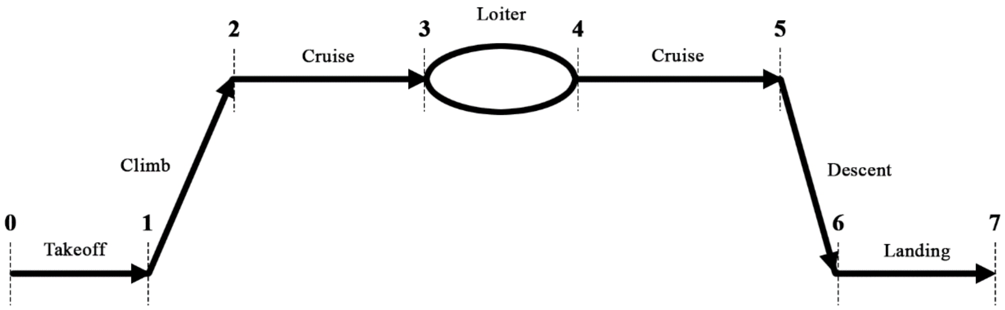

Figure 3.2 Mission profile of the aircraft

3.7.1 Takeoff Phase

The take-off phase covers the process from the moment the airplane starts moving on the runway until it reaches a certain velocity and altitude. The first weight estimate for this phase is as follows [3];

$$\frac{W_1}{W_0} = 0.97 \ to \ 0.99 \tag{3.62}$$

The take-off distance is expressed by [3] as follows;

$$\frac{W}{S} = TOP\sigma \frac{C_{l\,max}}{1.21}\left(\frac{hp}{w}\right) \tag{3.63}$$

Where takeoff parameter is expressed by [3] as follows;

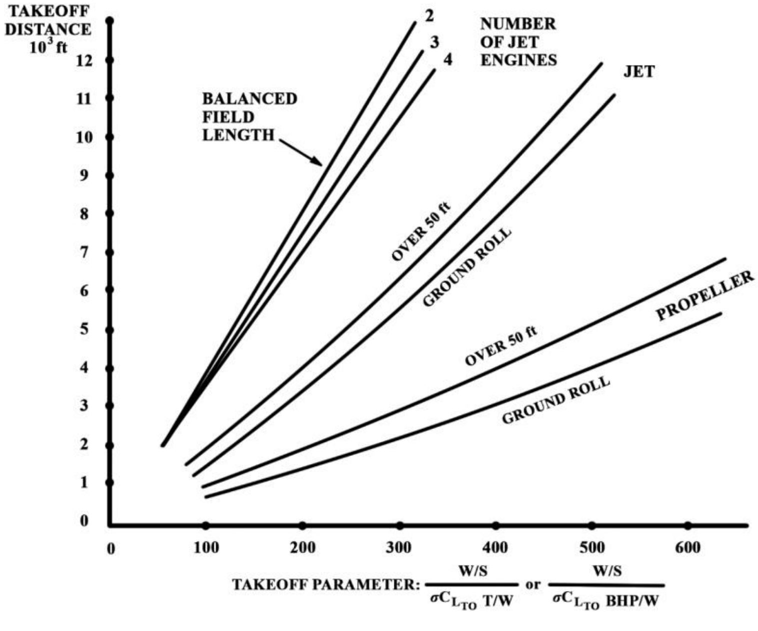

Figure 3.3 TOP vs takeoff distance [3].

3.7.2 Climb Phase

Climbing is the process of increasing the altitude of the aircraft until it reaches a specified cruising altitude. It comes before the aircraft reaches the cruise phase and after takeoff.

The equation for the climbing phase is as follows [3];

$$\frac{W_2}{W_1} = 0.985 \tag{3.64}$$

3.7.3 Cruise Phase

Cruise is the flight phase that comes at a constant altitude and speed, after reaching a certain altitude and before the descend phase begins. The aircraft achieves the most fuel efficiency at this stage.

As shown in the mission profile, the relevant equations for this phase 2-3 and 4-5 are as follows [3];

$$\frac{W_3}{W_2} = exp\left[\frac{-RC_{bhp}}{550\eta_p\left(\frac{L}{D}\right)_{max}}\right] \tag{3.65}$$

$$\frac{W_5}{W_4} = exp\left[\frac{-RC_{bhp}}{550\eta_p\left(\frac{L}{D}\right)_{max}}\right] \tag{3.66}$$

3.7.4 Loiter Phase

The loiter is the flight process in aviation that consists of an airplane traveling or flying over a certain small area.

The equation for the loiter phase is as follows [3];

$$\frac{W_4}{W_3} = exp\left[\frac{-EVC_{bhp}}{550\eta_p\left(\frac{L}{D}\right)}\right] \tag{3.67}$$

$$\left(\frac{L}{D}\right) = 0.866\left(\frac{L}{D}\right)_{max} \tag{3.68}$$

3.7.5 Descent Phase

The descent phase is the phase in which the aircraft decreases its altitude before landing. The equation for the descending stage is as follows [3];

$$\frac{W_6}{W_5} = 0.995 \tag{3.69}$$

3.7.6 Landing Phase

Landing is the last part of the flight where an airplane returns to where it completes its mission profile. The equation regarding the landing phase is given below [3];

$$\frac{W_7}{W_6} = 0.992 \text{ to } 0.997 \tag{3.70}$$

CHAPTER IV

INITIAL DESIGN AND CALCULATIONS

4.1 Airfoil Selection

The wing profile is the heart of the aircraft, which affects many aspects of aircraft performance and must be chosen carefully in design. It is the most important factor affecting the stall speed, cruising speed, usage characteristics, take-off, and landing distances, to summarize the aerodynamic efficiency of the aircraft during the flight process. Due to the relative motion between a moving airplane wing in the air and the air, drag and lift forces, which are aerodynamic forces, is generated. Airfoil NACA 63-412 (as shown in Figure 4.1) was chosen by taking into account Re, M and $C_{l\ design}$ parameters.

$$Re = \frac{U \times \bar{c}}{v} \tag{4.1}$$

$$M = \frac{u}{\alpha} \tag{4.2}$$

$$C_{l\ design} = \frac{w}{S_{ref}q} \tag{4.3}$$

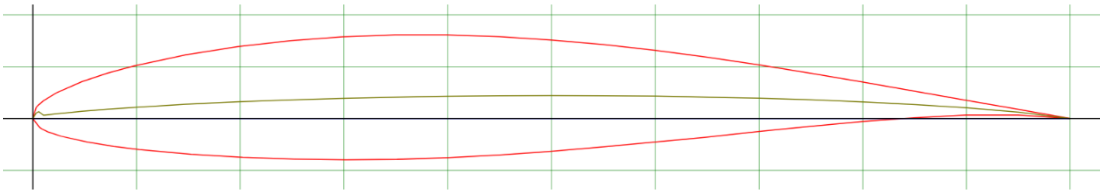

Figure 4.1 Naca 63-412

Airfoil thickness ratio has a critical effect on some parameters such as maximum lift, structural weight, drag, and stall characteristics. In Table 4.1, similar airfoils were compared according to the above parameters.

Table 4.1 Similar airfoils comparison table

Airfoils	Reynolds #	$C_{l_{\alpha=0}}$	$\left(C_L/C_D\right)_{max}$	Max. thickness
NACA 63-412	500,000	0.3381	99.8 at α=5°	12%
HQ 2.0/12	500,000	0.2720	90.7 at α=4.25°	12%
LDS-2	500,000	0.2330	97.7 at α=4°	12%
PSU-90-125WL	500,000	0.3307	87.8 at α=5.25°	12.5%
E195	500,000	0.3295	105.19 at α=5.25	11.8%
GOE 548	500,000	0.2715	94.96 at α=3.5°	11.9%

4.2 Calculation of Wing Loading

The term wing load, which has effects on take-off and landing distances, stall speed, turn performance, and rate of climb, is found by dividing the aircraft weight by the reference wing area. While wing load is including in the design, all flight conditions should be considered. Because the wing load directly refers to the lift coefficient.

When a larger wing is designed to increase aircraft performance, the wing load is reduced. However, this causes drag and empty weight, thus increasing the aircraft take-off gross weight. In the initial design stage, thrust-to-weight ratio and wing load should be optimized to the optimum value [3].

4.2.1 Stall Velocity Constraint

The theoretical calculation of V_{stall} is given below [3];

$$W = L = q_{stall} S C_{L_{max}} = \frac{1}{2} \rho V_{stall}^2 S C_{L_{max}} \tag{4.4}$$

$$V_{stall} = \sqrt{\frac{2\left(\frac{W}{S}\right)}{\rho C_{L_{max}}}} \tag{4.5}$$

4.2.2 Cruise Speed Constraint

Cruise speed calculation is as follows [55];

$$\frac{L}{D} = \left(\frac{\rho V^2 C_{D0}}{2\left(\frac{W}{S}\right)} + \frac{2K}{\rho V^2} \times \frac{W}{S}\right)^{-1} \tag{4.6}$$

4.2.3 Landing Run Constraint

The calculation of landing run constraint is as follows [3];

$$S_{landing} = 80\left(\frac{W}{S}\right)\left(\frac{1}{\sigma Cl_{max}}\right) + S_a \tag{4.7}$$

4.3 Calculation of Thrust to Weight Ratio

4.3.1 Takeoff Distance Constraint

The two-phase take-off distance is first the ground run and then the distance between it until it is 50 ft (35 ft commercial aircraft) where the wheels leave the ground. The sum of these two parameters gives the take-off distance.

The following [3] equation gives the calculation of the parameter;

$$\frac{W}{S} = TOP\sigma \frac{C_{l\,max}}{1.21}\left(\frac{hp}{w}\right) \tag{4.8}$$

The take-off speed of an aircraft is 1.1 times the stall speed. For this reason, the take-off lift coefficient is calculated by dividing the maximum take-off lift coefficient by 1.21 [3].

4.3.2 Cruise Speed Constraint

The parameter is calculated using the following equation [55];

$$\left(\frac{P}{W}\right)_{cruise} = \frac{1}{\left(\frac{L}{D}\right)_{cruise}} \tag{4.9}$$

4.3.3 Maximum Speed Constraint

Maximum speed constraint has been calculated using [45] the following equation;

$$V_{max} = \left\{ \frac{\left[\frac{T_{A\,max}}{W}\right]\left(\frac{W}{S}\right) + \left(\frac{W}{S}\right)\sqrt{\left[\frac{T_{A\,max}}{W}\right]^2 - 4C_{D0}K}}{\rho C_{D0}} \right\} \tag{4.10}$$

$$T_{A\,max} = \frac{\eta P_{A\,max}}{V} \tag{4.11}$$

4.4 Engine Selection

Engine selection was made by considering certain criteria, especially the compatibility of T/W ratio with engine power. For this reason, the PBS TP100 Turboprop engine has been selected, which has high efficiency at low speeds, accelerates the outside air with a propeller, and realizes the mechanical power through a turbine. In the study, it was preferred to be used only in designs made for unmanned aerial vehicles.

Table 4.2 Specifications of PBS TP100 turboprop engine [56].

Output shaft speed	2,158 RPM
Power supply	28 V DC
Electrical power output	720 W
Take-off	180 kW (241 HP)
Max. continuous	160 kW (214 HP)
Cruise	140 kW (188 HP)
Height x width - without exhaust	398 x 330 mm
Length	891 mm
Weight	61.6 kg
Gas generator speed - 100%	56,200 RPM
Max. operating altitude	0 m to 9,000 m (0 ft to 29,500 ft)
Max. starting altitude	0 m to 6,000 m (0 ft to 19,700 ft)

4.5 Propeller Sizing

During the design process, the dimensions of the engine, the diameter of the propeller, the required inlets and exhaust should be determined. Increasing the propeller diameter also increases efficiency.

As expressed in the following equation, the propeller tip velocity is obtained by the sum of the rotational speed vectorially [3];

$$\left(V_{tip}\right)_{static} = \frac{\pi n d}{60} \quad (ft/s) \tag{4.12}$$

Where d is the diameter and n is the rotational rate (rpm).

The forward speed of the aircraft is given in the equation below [3];

$$\left(V_{tip}\right)_{helical} = \sqrt{V_{tip}^2 + V^2} \tag{4.13}$$

The following equation expresses an estimate of the three blade propeller diameter [3];

$$d = 18\sqrt{Hp} \tag{4.14}$$

4.6 Wing and Fuselage Design

4.6.1 Wing Design

Wing parameters such as aspect ratio, taper ratio, span, wingtip, dihedral and sweep angle, wing vertical position, twist are very important for aircraft performance.

The taper ratio λ, is calculated by dividing the root by the tip chord. Normally, most wings with a taper ratio of 0.4-0.5 have a low sweep angle. The taper ratio has a great effect on the lift distribution along the wingspan. Manufacturing an elliptical wing is an expensive and difficult process. For this reason, a rectangular wing design with a taper ratio of 0.43 that provides the same lift distribution as an elliptical wing is preferred. The wing twist is applied in the design to bring the lift distribution closer to the elliptical wing type and to prevent the wingtip from stalling [3].

The angle of incidence of the airfoil changes with the geometric twist. Wingtip airfoil is expressed as "wash out" when there is a less angle of incidence compared to the root airfoil. When the twist is increased to reach the elliptical wing lift distribution with the desired improvement, the efficiency of the wing at different angles of attack decreases [3]. To summarize, when the lift distribution is done by twist, it has an effect on a single lift coefficient.

The effect of the dihedral wing for the aircraft can be expressed as stability. As the angle of the wing with the horizontal axis increases, the stability increases, however, the maneuverability decreases [55].

4.6.2 Fuselage Design

The fuselage is the main compartment of an aircraft that carries loads that include crew, passengers, or cargo. Body sizes may vary for different aircraft types, but contain limited design rules for some classes of aircraft. For example, for a cargo plane, most of the fuselage length is reserved for the cargo compartment.

Fuselage length calculation is given with the following formula [3];

$$l_f = \alpha . W_0^c \quad (4.15)$$

Where the coefficients α and c are variables depending on the aircraft type and W_0 are the aircraft take-off gross weight in lbs.

4.6.3 Winglet Geometry Selection

Winglets are design extensions that are generally positioned perpendicular to the wingtips, which are used to increase the efficiency of the aircraft by reducing the induced drag, and also have a positive effect on the lift and drag ratio [25].

The holding of an aircraft in motion occurs due to the pressure difference under the wing created by the lift force acting on the aircraft. The pressure difference causes the flow over the wing to form vortex as it leaves the wing [57]. The size of the vortexes formed may differ according to the aircraft wing type, speed, and weight.

The use of winglets has a positive effect on the aircraft's climbing performance, range, and ceiling height. It also causes the aircraft to fly quieter and the engine to work more efficiently.

4.7 Fuel Space Calculation

The calculations made at this stage have been made considering that the flow type is only air due to the motor selection.

Trapped fuel calculation is expressed as follows [3];

$$\frac{W_f}{W_0} = 1.06\left(1 - \frac{W_x}{W_0}\right) \tag{4.16}$$

Then, the calculation of the fuel volume is given below;

$$V_f = \frac{W_f}{\rho_f} \tag{4.17}$$

4.8 Landing Gear Locating and Sizing

The landing gear is the undercarriage of an aircraft or UAV used during take-off, landing, or taxiing.

The most used landing gear layout today is the tricycle landing gear with two main wheels at the rear and an auxiliary wheel at the front. This landing gear layout used in the UAV designed in this study is fixed to the ground since the center of gravity is in front of the main wheels.

The design of landing gear is often the part of the aircraft layout that causes the most problems of most components that need to be identified. Positioning the landing gear at the right angle and position is important as it includes the installation of other subsystems. Attention should be paid to tail tipping at this stage, so the tipback angle should be at least 15^o. The following equations give the correct sizing, placement of the landing gear, calculation of the tail down and tipback angle [3];

$$tan\theta_{static\ taildown} = \frac{H_2}{x_{main\ landing\ gear}} \tag{4.18}$$

$$tan\theta_{tipback} = \frac{x_{cg\ aircraft} - x_{main\ landing\ gear}}{H_1} \tag{4.19}$$

$$x_n = x_{cg\ wing} - x_{nose\ gear\ location} \tag{4.20}$$

$$x_m = x_{main\ landing\ gear} - x_{cg\ aircraft} \tag{4.21}$$

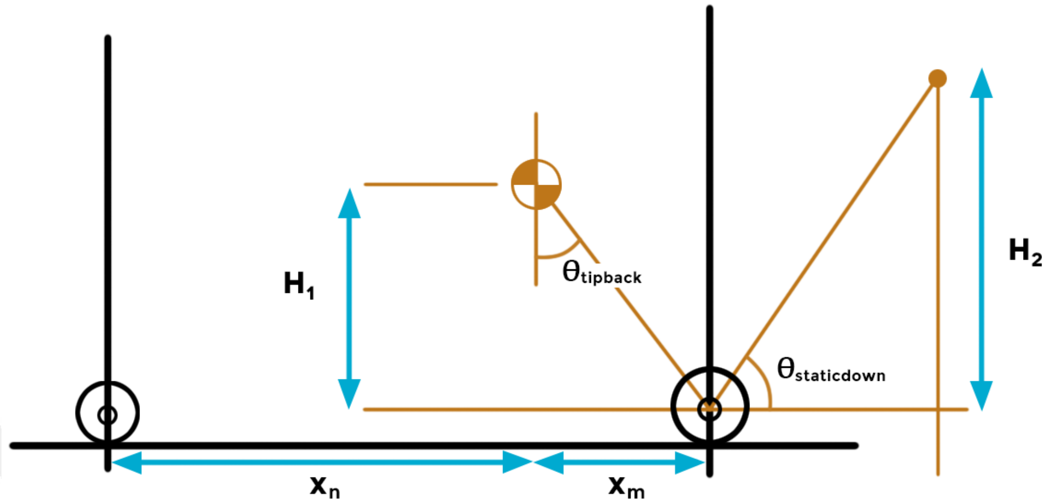

Figure 4.2 Location of landing gears [3].

The following equations are given for nose landing gear sizing;

$$F_n(x_n + x_m) = W_0\left(x_{cg\ wing} - x_{cg\ aircraft} - x_m\right) \tag{4.22}$$

The following equations are given for main landing gear sizing;

$$2F_m(x_n + x_m) = W_0\left(x_{cg\ aircraft} - x_{nose\ gear\ location}\right) \tag{4.23}$$

The wheel width and diameter for the nose landing gear are as follows;

$$D_{nose} = A(W_n)^B \tag{4.24}$$

The wheel width and diameter for the main landing gear are as follows;

$$D_{main} = A(W_m)^B \tag{4.25}$$

Where A and B values are selected according to general aviation studies.

The retraction of the landing gear is chosen for the designed concept UAV, as it aerodynamically reduces the drag coefficient.

4.9 Aerodynamic Analysis

In this section, aerodynamic characteristics and external geometry calculations of the designed UAV are calculated step by step and given in Table 4.3.

4.9.1 Outer Geometry Calculations

Table 4.3 Aircraft geometrical specifications

Taper Ratio	0.43	Fuselage Width (m)	0.5
Wing Span (m)	6.75	Fuselage Length (m)	5
Aspect Ratio	10.3	$S_{wet.fuselage}$ (m^2)	5.52
Sweep Angle (°)	0°	S_{wing} (m^2)	9.97
Vertical Tail Root Chord (m)	1.34	S_{wet} (m^2)	17.70
Vertical Tail Tip Chord (m)	0.24	$S_{exp.wing}$ (m^2)	4.43
Vertical Tail Span (m)	0.63	$S_{exp.V.T}$ (m^2)	0.38
Horizontal Tail Root Chord (m)	0.75	$S_{exp.H.T}$ (m^2)	1.12
Horizontal Tail Tip Chord (m)	0.25	Horizontal Tail Sweep (°)	27°
Wing Dihedral (°)	15°	Vertical Tail Sweep (°)	63°

The dimensions of the UAV designed in Figure 4.3 are shown on the front, top and side views.

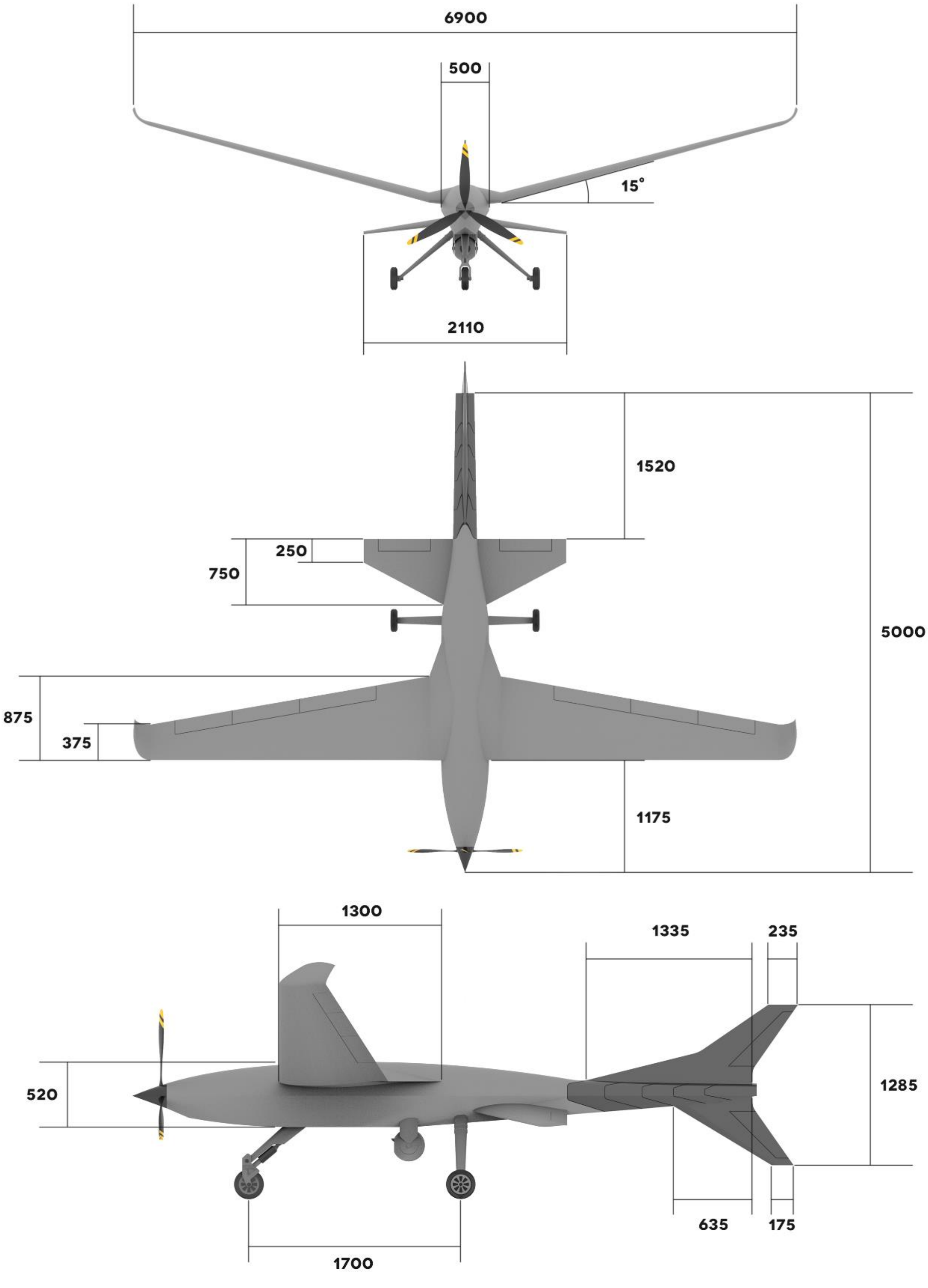

Figure 4.3 Aircraft final geometry dimensions in mm

CHAPTER V

COMPUTATIONAL APPROACH

In this part of the study, CFD analysis was performed at different wing angles in order to create a more aerodynamically efficient UAV design.

5.1 Numerical Analysis

In recent years, CFD tools are widely used in the design, analysis, and optimization stages. With the use of computational flow simulation tools, it has become more convenient for engineers to verify their designs. Considering parameters such as cost reduction, the efficiency of the time required for design, optimization, and modeling, computer aided tools are of great importance to obtain accurate results [58].

In the first step, the 3D geometric model of the UAV was designed in detail in Solidworks and rendered in Keyshot, as shown in Figure 5.1 and Figure 5.2.

Figure 5.1 3D rendering of the UAV (front perspective)

Figure 5.2 3D rendering of the UAV (back perspective)

Then, 3D models of the specified wing configurations were created to perform flow analysis at 0°, 5°, 10°, 15° wing angles. Figure 5.3 below shows the 0° wing angle design with NACA 63-412 airfoil. The wing has a length of 3 meters.

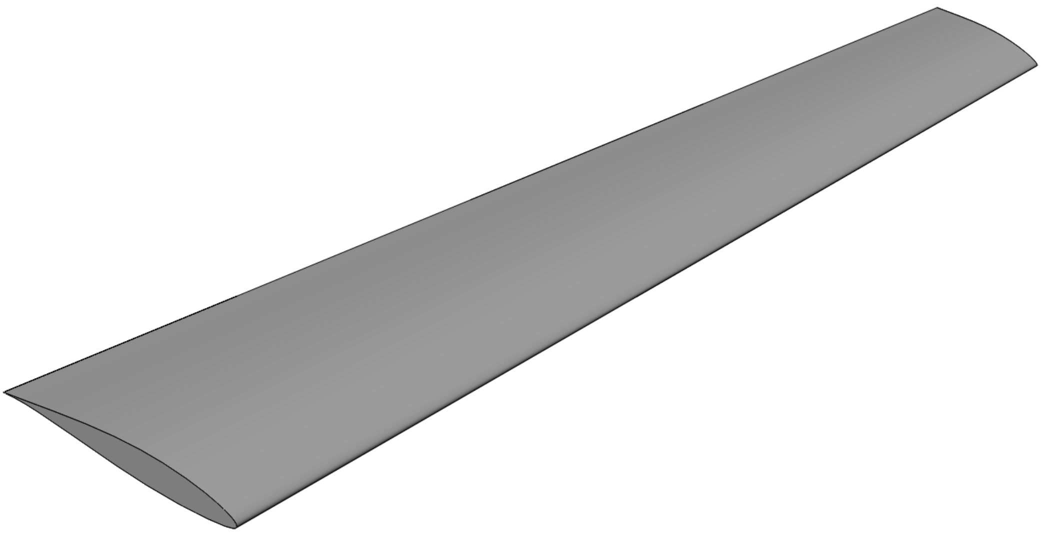

Figure 5.3 3D model of the wing angle at 0°

The designed wing has a tip chord of 0.375 m and a root chord of 0.875 m. By positioning the wing to the UAV body high, a connection element with a 1.3 m root chord continuing with the same wing profile was designed.

5.2 Mesh Generation

The use of CFD tools is efficient in terms of increasing the design span, working in harmony with similar tools, reducing the risk in the design process, and reproducibility of the design.

Solidworks Flow Simulation, a CFD tool, was used for numerical calculations and aerodynamic analysis for the designed unmanned aerial vehicle and its configurations. After the 3D model was created in the program, the mesh creation process was performed. The mesh model of the UAV wing is as shown in Figure 5.4 at 0° wing angle.

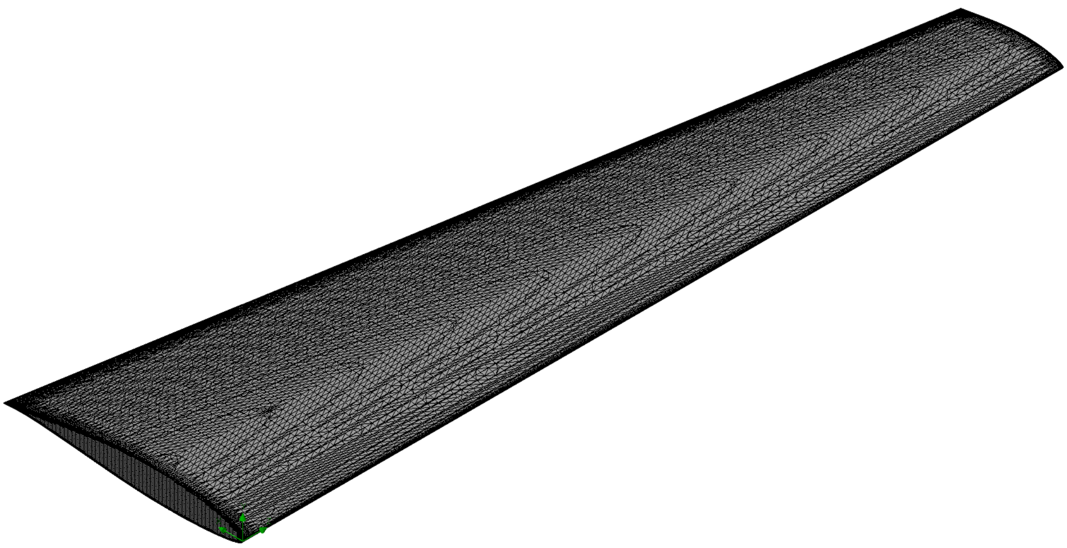

Figure 5.4 Mesh model of the wing angle at 0°

Mesh settings were used on the model with the appropriate minimum gap size, correct curvature refinement level, and minimum wall thickness [59]. The solution time of the program is largely related to the number of cells in the calculation area. While creating the mesh in Solidworks Flow Simulation, a compute volume divided into blocks was created using the finite volume method.

Spikes, slivers, faces, and sharp angles have been renovated for computational results and accurate meshing. Afterward, the control volume was sized by considering the flow so that it did not reach the surface boundaries of the 3D model wing. The larger the control volume is set when performing CFD analysis, the more reliable the result.

Body geometry, flow type, flow velocity, mesh type, and viscosity are important parameters for computation area sizing.

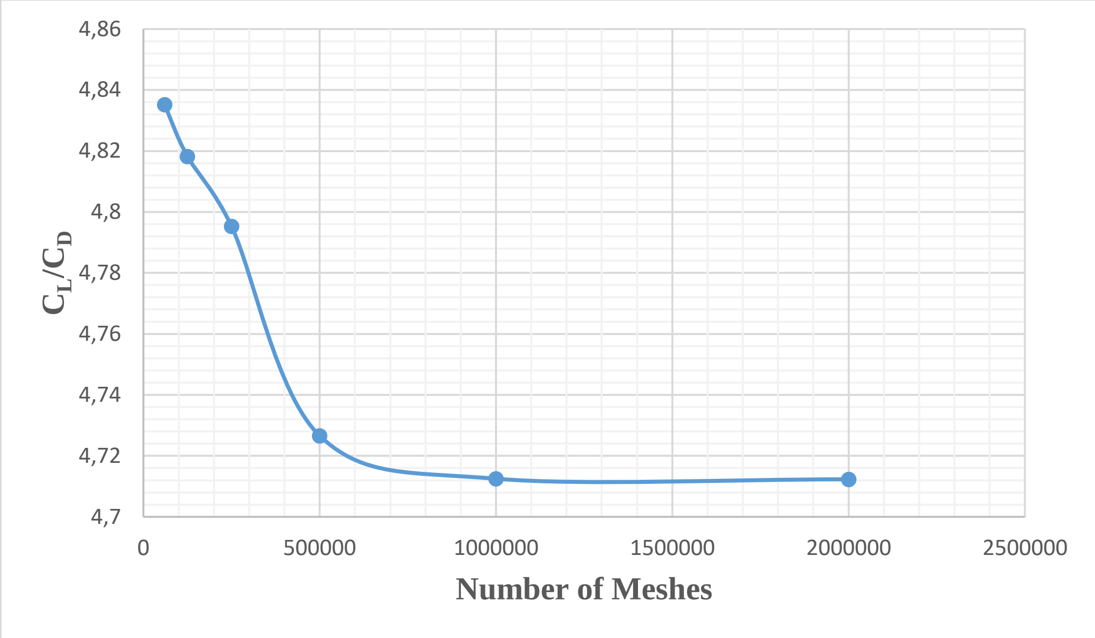

Figure 5.5 Mesh independence study results

The results obtained by using different mesh values in the mesh independence test, which is also expressed as the grid convergence in the study, are compared and shown in Figure 5.5. The results show that mesh numbers above 1.000.000 will be unnecessary.

5.3 Numerical Method and Boundary Conditions

Solidworks Flow Analysis software based on the finite volume method is used for numerical calculations. Gravity was neglected and pressure based and 20° temperature was chosen for the analysis method. The density of the air is 1.19 kg/m^3 and the free flow velocity is assumed to be 50 m/s. The flow type is chosen as laminar and turbulent. All the above parameters are applied for setting up simulations.

CHAPTER VI

RESULTS AND DISCUSSION

In this section, the lift and drag forces of the designed UAV wing were calculated using CFD analysis at different wing angles. In addition to these parameters, the effects of changing the wing angle on static pressure, velocity, and vorticity were investigated.

6.1 Analysis Results

Static pressure, velocity, and vorticity results were as shown in Figure 6.1, Figure 6.2, and Figure 6.3 for the UAV wing angle at 0°.

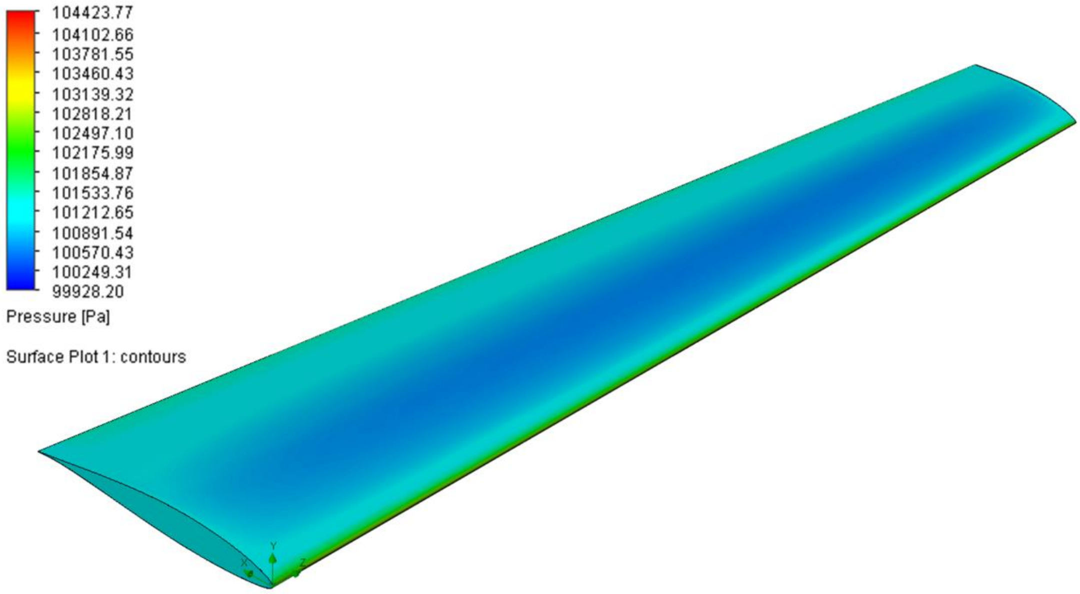

Figure 6.1 Pressure (Pa) value of the wing angle at 0°

After performing the analysis, the computational domain in the positive X direction was used as the starting point for the flow to generate the flow trajectory chart. 200 trajectories were created in the study. Since the flow analysis was performed covers a certain computational domain, the resulting images give limited detail.

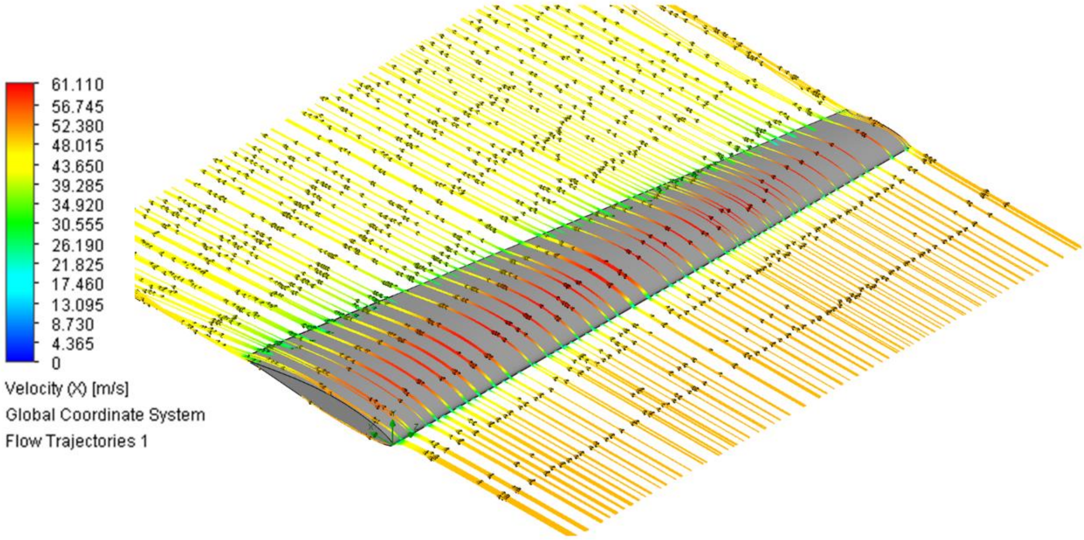

Figure 6.2 Velocity (m/s) value of the wing angle at 0°

In the figure above, velocity flow trajectories occurring against the flow of 50 m/s around the 0° wing are seen. It was seen that the flow reaches maximum speed on the upper surface of the wing and slows down as it leaves the wing.

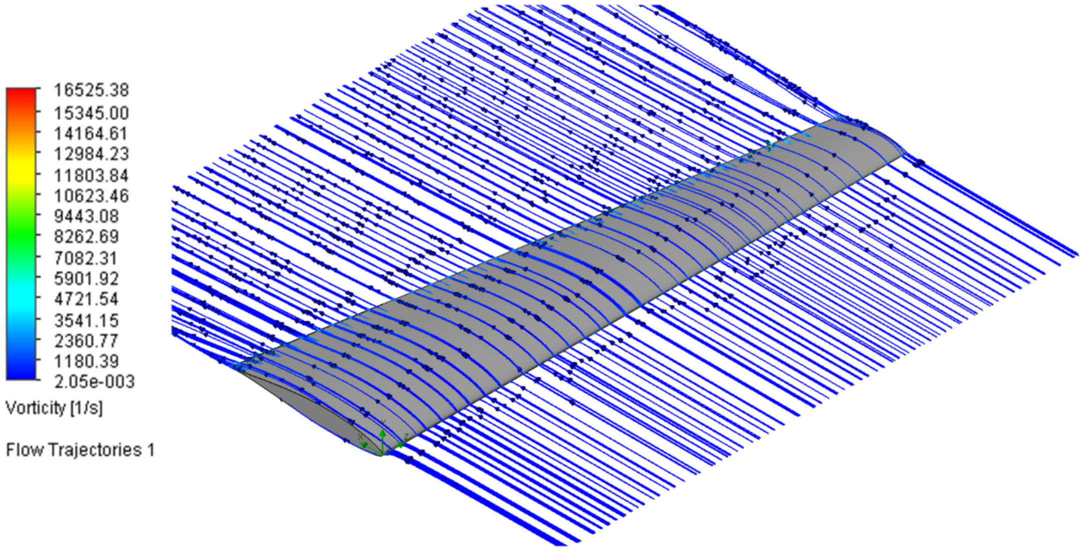

Figure 6.3 Vorticity (1/s) value of the wing angle at 0°

As observed in the analysis the vorticity flow trajectories as they leave the wingtip and apply downward force to the wing. This situation causes a vortex behind the wing. In order to avoid this type of flow that occurs, aerodynamic improvement will be realized by designing curved wingtip geometry after the analysis is completed.

Static pressure, velocity, and vorticity results were as shown in Figure 6.4, Figure 6.5, and Figure 6.6 for the UAV wing angle at 5°.

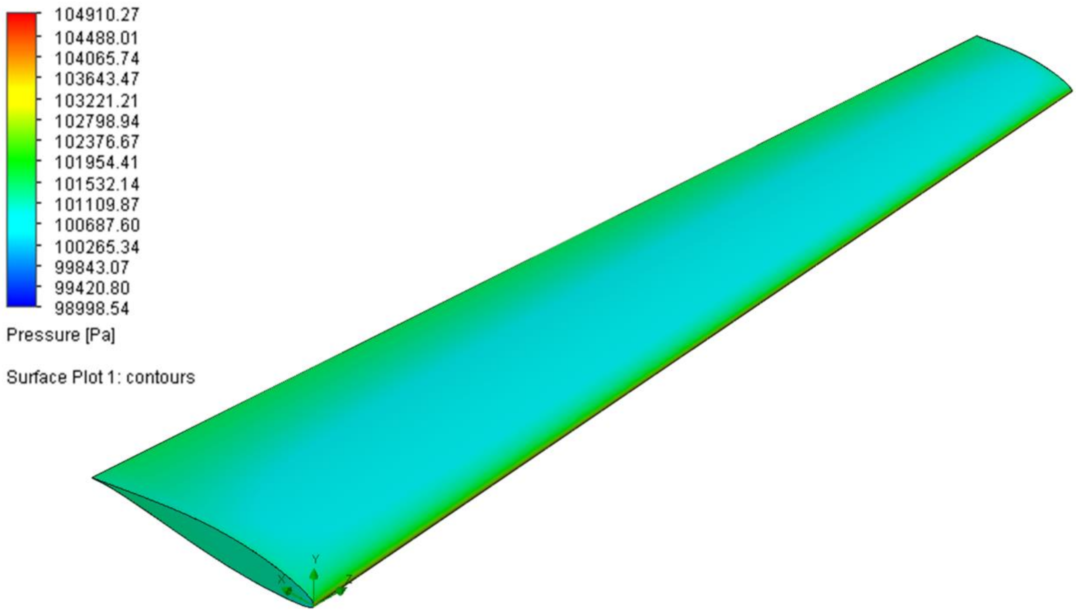

Figure 6.4 Pressure (Pa) value of the wing angle at 5°

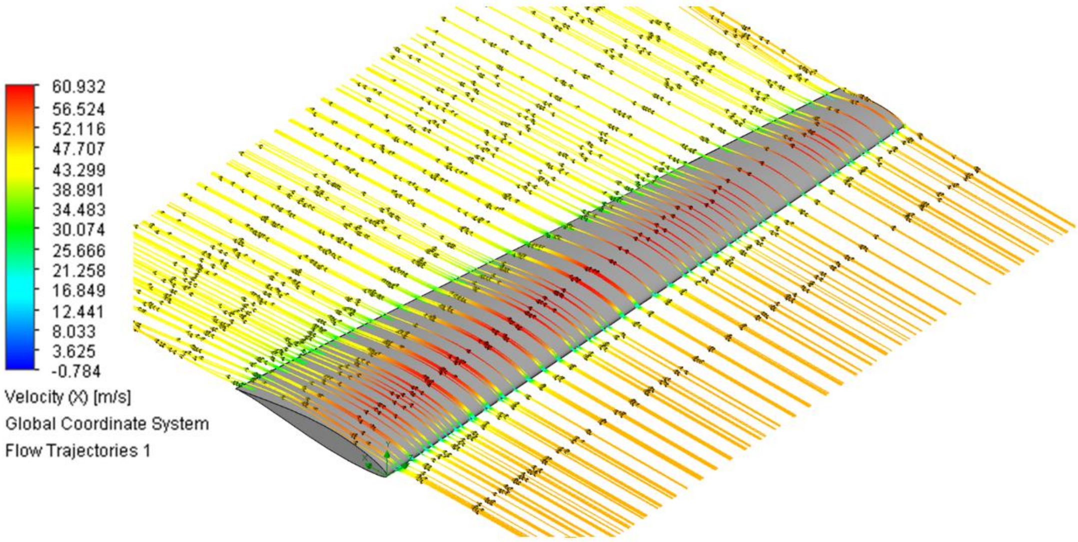

Figure 6.5 Velocity (m/s) value of the wing angle at 5°

It was observed that the velocity flow trajectories formed at 5° wing angle reached the maximum speed on the upper surface of the wing again due to the wing profile. However, this speed was relatively lower than the maximum speed at 0° wing.

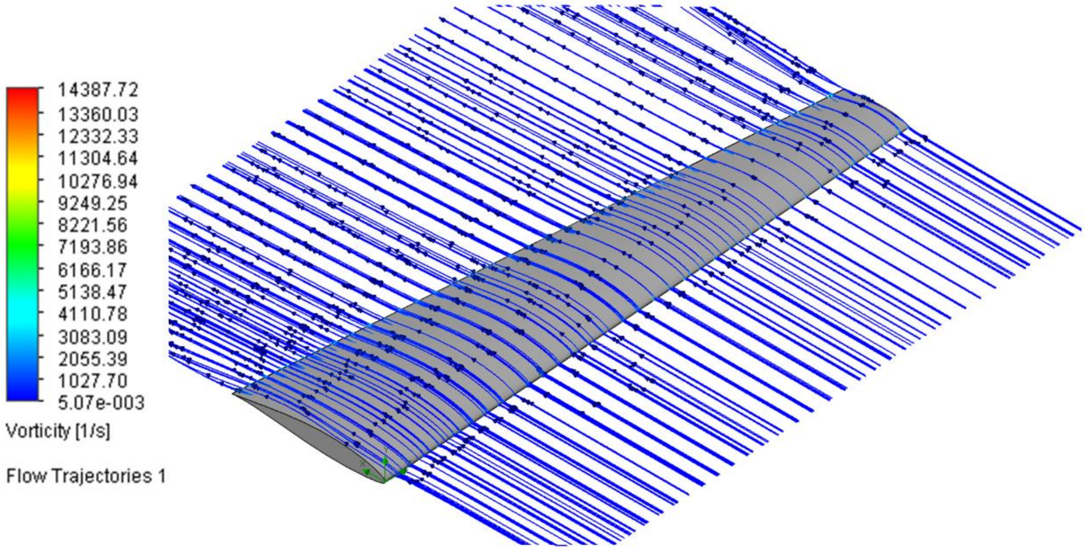

Figure 6.6 Vorticity (1/s) value of the wing angle at 5°

Static pressure, velocity, and vorticity results were as shown in Figure 6.7, Figure 6.8, and Figure 6.9 for the UAV wing angle at 10°.

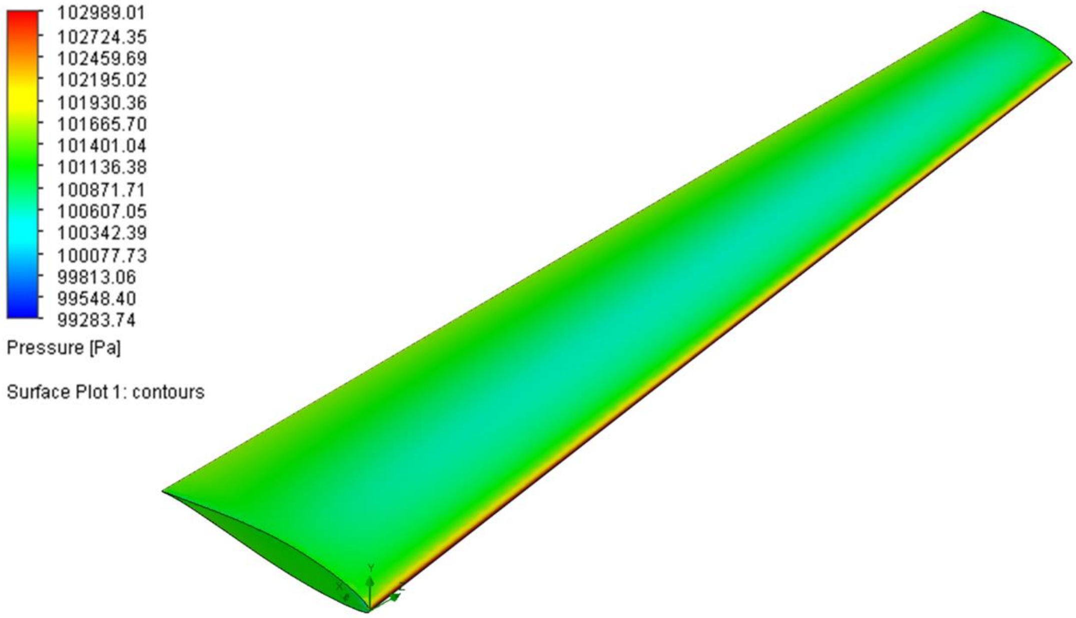

Figure 6.7 Pressure (Pa) value of the wing angle at 10°

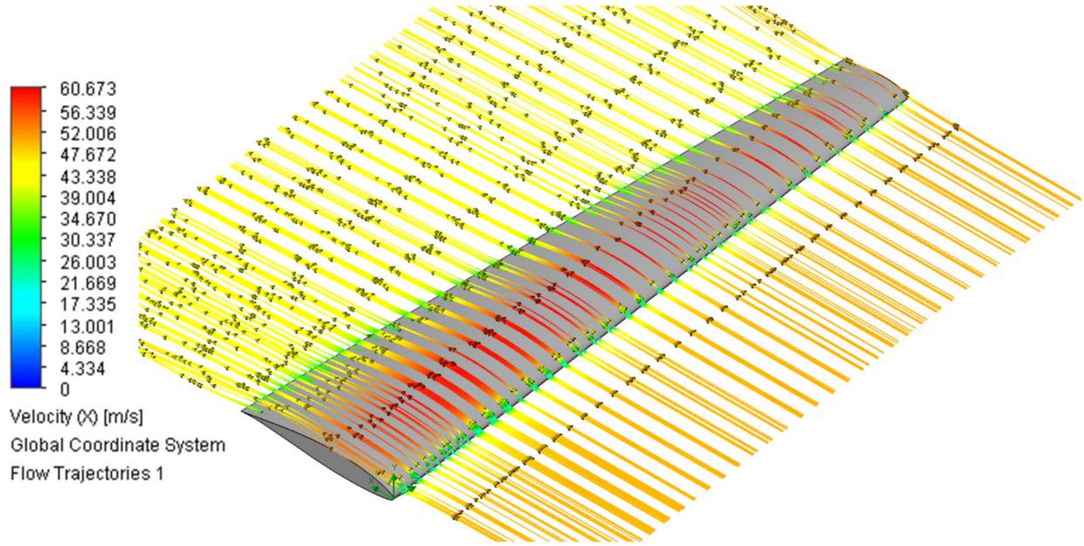

Figure 6.8 Velocity (m/s) value of the wing angle at 10°

The velocity flow trajectories were formed at 10° wing angle to reach the maximum speed above the wing after the first impact on the wing. Results obtained from trajectory plots can be informative in terms of flow visualization.

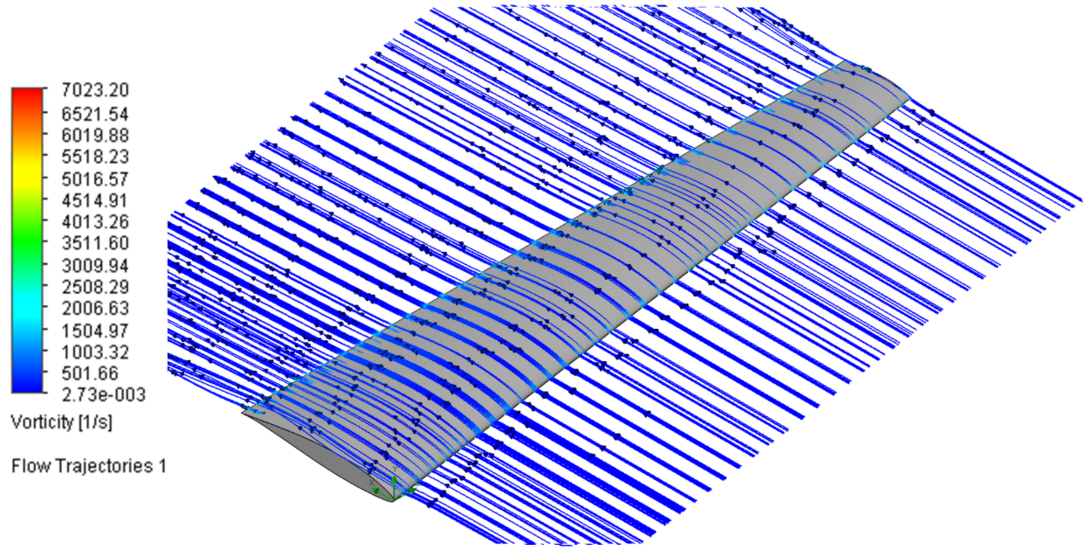

Figure 6.9 Vorticity (1/s) value of the wing angle at 10°

Static pressure, velocity, and vorticity results were as shown in Figure 6.10, Figure 6.11, and Figure 6.12 for the UAV wing angle at 15°.

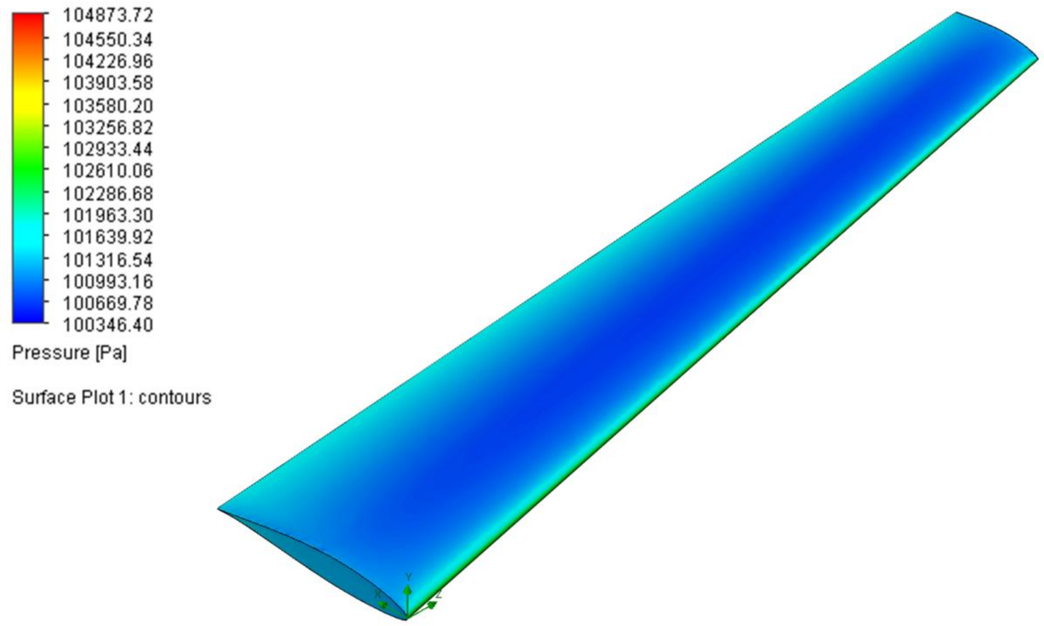

Figure 6.10 Pressure (Pa) value of the wing angle at 15°

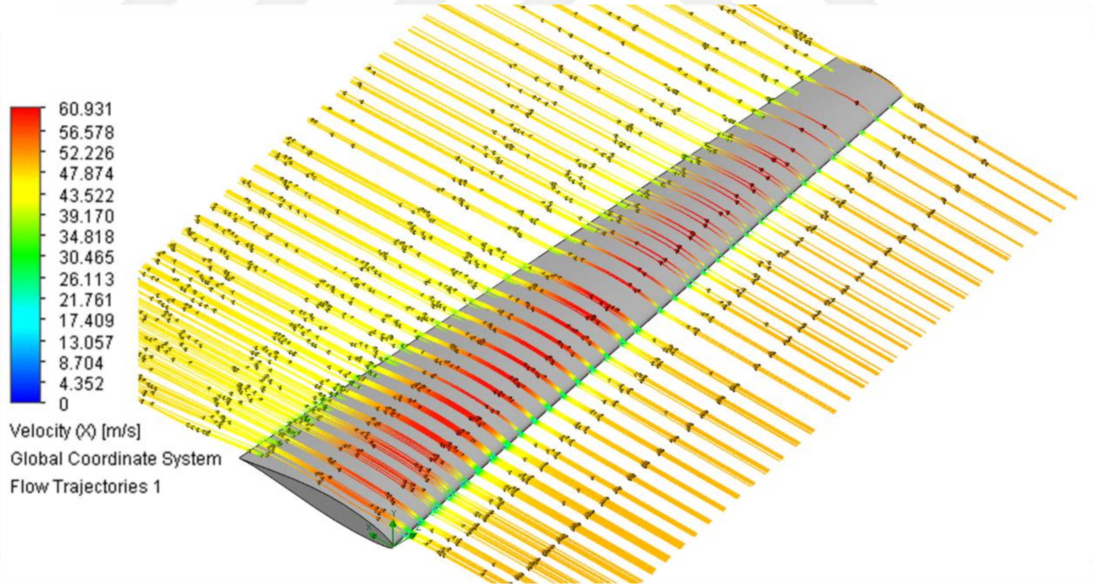

Figure 6.11 Velocity (m/s) value of the wing angle at 15°

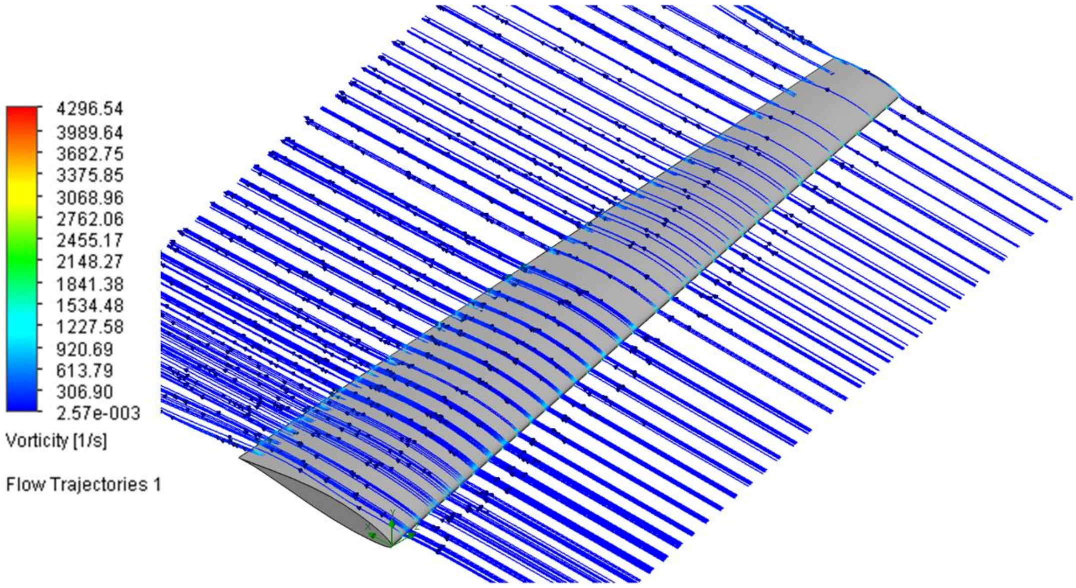

Figure 6.12 Vorticity (1/s) value of the wing angle at 15°

6.2 Calculation of Aerodynamic Coefficients

The lift coefficient (C_L) and drag coefficient (C_D) values were as shown in Table 6.1, C_L/C_D ratios are as shown in Table 6.2, and lift force and drag force values are as shown in Table 6.3 respectively. Also, the lift and drag force graphic is shown in Figure 6.13 and the graph of C_L/C_D ratio is shown in Figure 6.14.

Table 6.1 C_L and C_D values according to wing angle for 0° angle of attack

Wing Angle	**C_L**	**C_D**
0°	0.1833	0.0389
5°	0.1762	0.0392
10°	0.1771	0.0406
15°	0.1725	0.0419

Table 6.2 C_L/C_D ratio according to wing angle for 0° angle of attack

Wing Angle	**C_L/C_D**
0°	4.712
5°	4.495
10°	4.362
15°	4.117

The aspect ratio and taper ratio of the wing play a major role in creating the maximum lift force. In the analysis, with the increase of the wing angle, the reference area perpendicular to the flow direction was used in the drag coefficient calculation decreases. However, as the angle of attack increases, this area increases. This situation causes more resistance to flow.

Table 6.3 Drag and lift force according to wing angle for 0° angle of attack

Wing Angle	**Drag Force (N)**	**Lift Force (N)**
0°	13.161	513.648
5°	13.208	491.667
10°	13.506	488.668
15°	13.677	466.496

Similarly, as the wing angle increases, the reference wingspan area used for the lift coefficient calculation decreases. This area decreases as the angle of attack increases. After the reference area values calculated in Solidworks are inserted into the equation, the other parameters required for the lift coefficient and drag coefficient calculations are lift force and drag force. These values were shown in the above tables are primarily given by assuming that the UAV is in cruise phase and at 0° angle of attack.

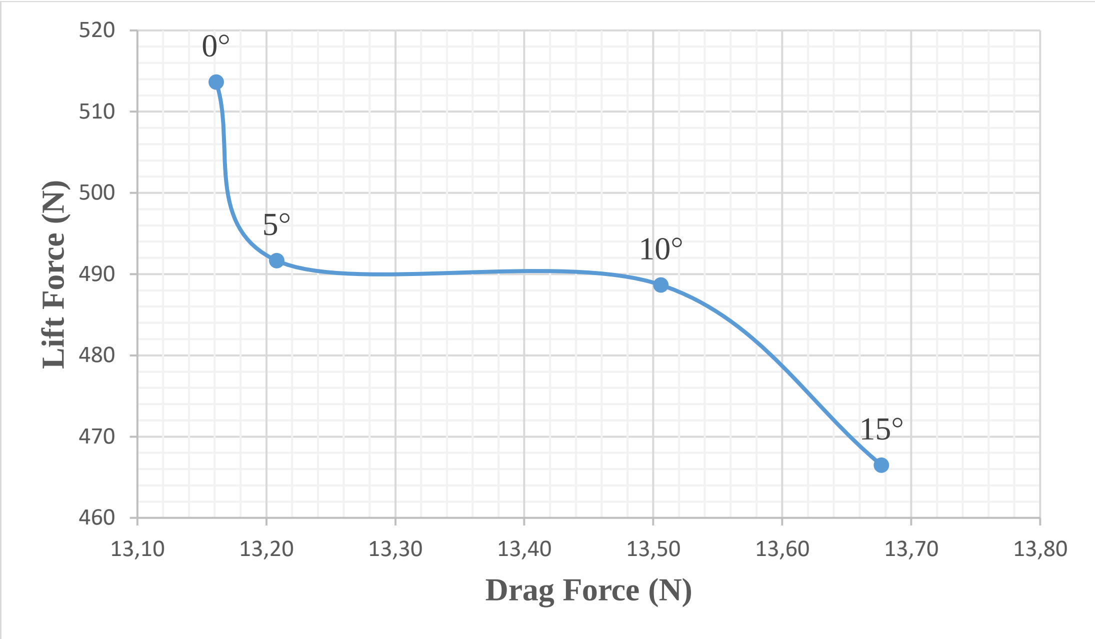

Figure 6.13 Drag and lift force according to wing angle for 0° angle of attack

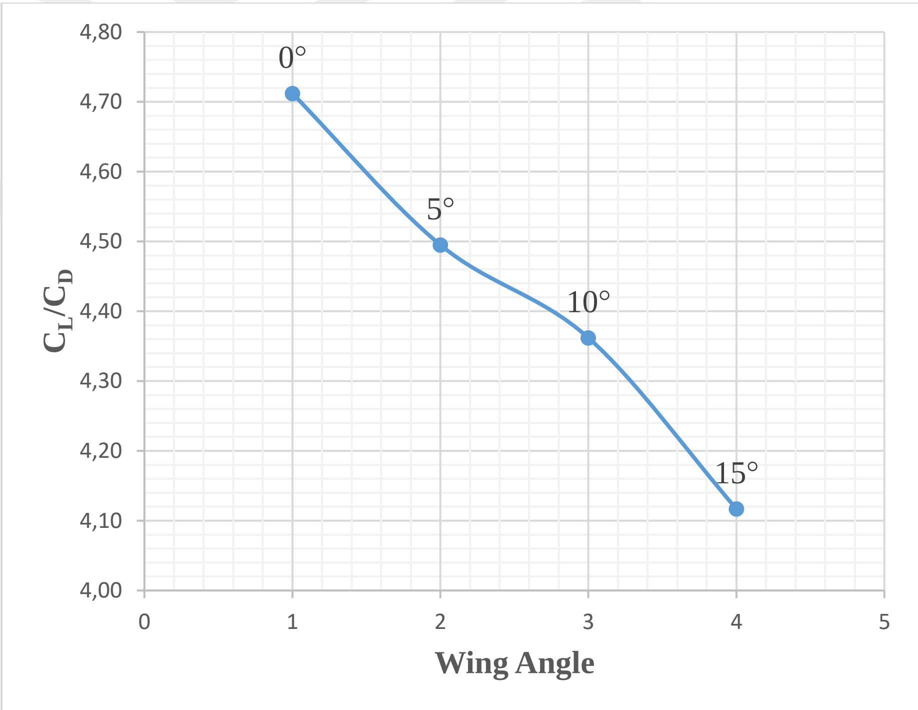

Figure 6.14 C_L/C_D ratio according to wing angle for 0° angle of attack

In Table 6.4, the lift coefficient values at 0°, 5°, 10°, and 15° wing angles were calculated and shown at different angle of attacks. During the calculation, the reference area was calculated and included in the equation at the wing angles specified with the increase of the angle of attack.

Table 6.4 C_L values according to angle of attack at each wing angle

Angle of Attack	**Wing Angle**			
	C_L at 0°	**C_L at 5°**	**C_L at 10°**	**C_L at 15°**
0°	0.1833	0.1762	0.1771	0.1725
2°	0.1842	0.1770	0.1780	0.1733
4°	0.1847	0.1774	0.1783	0.1736
6°	0.1852	0.1779	0.1789	0.1741
8°	0.1860	0.1787	0.1796	0.1748
10°	0.1870	0.1797	0.1807	0.1758

Drag coefficient values at 0°, 5°, 10°, and 15° wing angles were calculated in different angles of attack and given in Table 6.5. During the calculation, the reference area perpendicular to the flow direction was calculated and included in the equation at the wing angles specified with the increase of the angle of attack.

Table 6.5 C_D values according to angle of attack at each wing angle

Angle of Attack	**Wing Angle**			
	C_D at 0°	**C_D at 5°**	**C_D at 10°**	**C_D at 15°**
0°	0.0389	0.0392	0.0406	0.0419
2°	0.0385	0.0395	0.0410	0.0422
4°	0.0369	0.0375	0.0395	0.0398
6°	0.0305	0.0310	0.0321	0.0331
8°	0.0260	0.0264	0.0273	0.0281
10°	0.0226	0.0228	0.0236	0.0243

C_L/C_D ratio at 0°, 5°, 10° and 15° wing angles was calculated in different angles of attack and given in Table 6.6. These calculated values were shown on the graph in Figure 6.15.

Table 6.6 C_L/C_D ratio according to angle of attack at each wing angle

Angle of Attack	**Wing Angle**			
	C_L/C_D at 0°	**C_L/C_D at 5°**	**C_L/C_D at 10°**	**C_L/C_D at 15°**
0°	4.712	4.495	4.362	4.117
2°	4.784	4.481	4.341	4.107
4°	5.005	4.731	4.514	4.362
6°	6.072	5.739	5.573	5.260
8°	7.154	6.769	6.579	6.221
10°	8.274	7.882	7.657	7.235

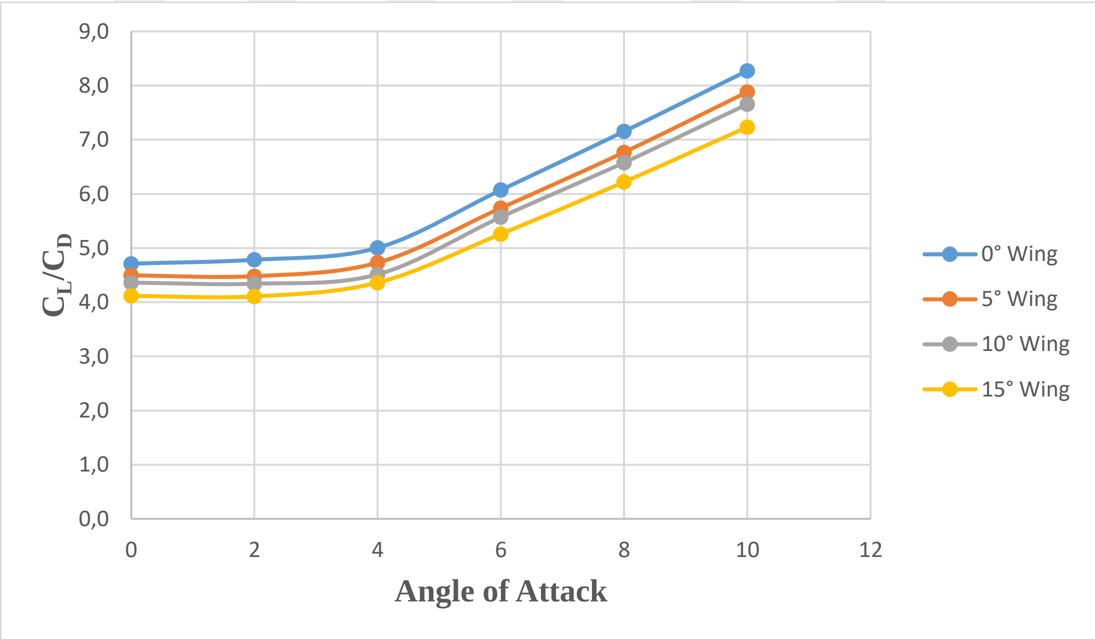

Figure 6.15 C_L/C_D ratio according to angle of attack at each wing angle

CHAPTER VII

CONCLUSIONS

In the study, a medium altitude UAV was designed with a conceptual approach, inspired by flying fish. The main features were determined for the UAV are cruising altitude over 5000 m, approximately 12 hours endurance, 150 km communication range, 100 kg payload, 6.75 m wingspan, 10.3 aspect ratio, 0.43 taper ratio. During the design process, historical experiences and equations were examined and various parameters and configurations were used to make the UAV's aerodynamic performance efficient. For example, wing types and positioning relative to the fuselage. Various calculations were made about the effects and coefficients of the designed wing geometry on the aerodynamic performance of the UAV. Then, the appropriate wingtip geometry was designed and vortex concentrations in the air have been avoided.

In the CFD analysis process, concept UAV wing models at 0°, 5°, 10°, and 15° angles were examined in terms of drag and lift force arising from aerodynamic forces, which are the most critical parameters at the design stage. Lift and drag forces on the three dimensional NACA 63-412 airfoil wing were analyzed at different wing angles.

When Figure 6.13 was examined, it was seen that the wing angle of 0° is more effective on the lift force for the UAV. At 0° the wing is about 4.5% better than the wing at 5°, about 5% better than the wing at 10°, and about 10% better than the wing at 15° in terms of the lift force.

Drag force is the critical parameter for fuel consumption in aircraft. When Figure 6.14 was examined, it was clear that the 0° wing is about 5% better than the 5° wing, 8% better than the 10° wing, and 14.5% better than the 15° wing.

As can be seen in Table 6.4, the lift coefficient increases at each wing angle with increasing angle of attack. When Table 6.5 was examined, the increase in the angle of attack causes a decrease in the drag coefficient for each wing angle. In addition, C_L/C_D ratios at each wing angle increase with increasing angle of attack, as given in Table 6.6. As a result, it was observed that the wing at 0° is more efficient than the wings at other angles calculated in this study with the increase of angle of attack as given in Figure 6.15.

The study was carried out by observing the structures and movements of flying fish, which is the subject of an idea with a different approach to aircraft designs made today. Aircraft designs must go through a very detailed design and optimization process in order to compete and stand out from their competitors in the aviation field.

In the aerodynamic optimization process, the aspect ratio, taper ratio, selected airfoil, sweep angle, and area are critical parameters. Completing such a process requires detailed calculation and teamwork. The aerodynamic optimization process was carried out in the thesis has been performed by assuming that the UAV wing is at different dihedrals at a certain cruising phase and at a constant angle of attack.

CHAPTER VIII

FUTURE WORKS

In a future study, a model of the unmanned vehicle designed for the air environment, inspired by flying fish, can be realized that can move underwater. Vehicles that can be used as traditional unmanned are designed and manufactured separately as air vehicle, underwater the vehicle, and land vehicle. In order for unmanned aerial vehicles to move underwater, it is necessary to have propulsion systems and direction control systems that are very different from those that they can move in the air.

Unmanned aerial or underwater vehicles produced with traditional designs are designed in such a way that there is no problem in performing their duties due to their different categories. However, it does not seem possible for unmanned vehicles in these two different categories to perform tasks in the same category with conventional design.

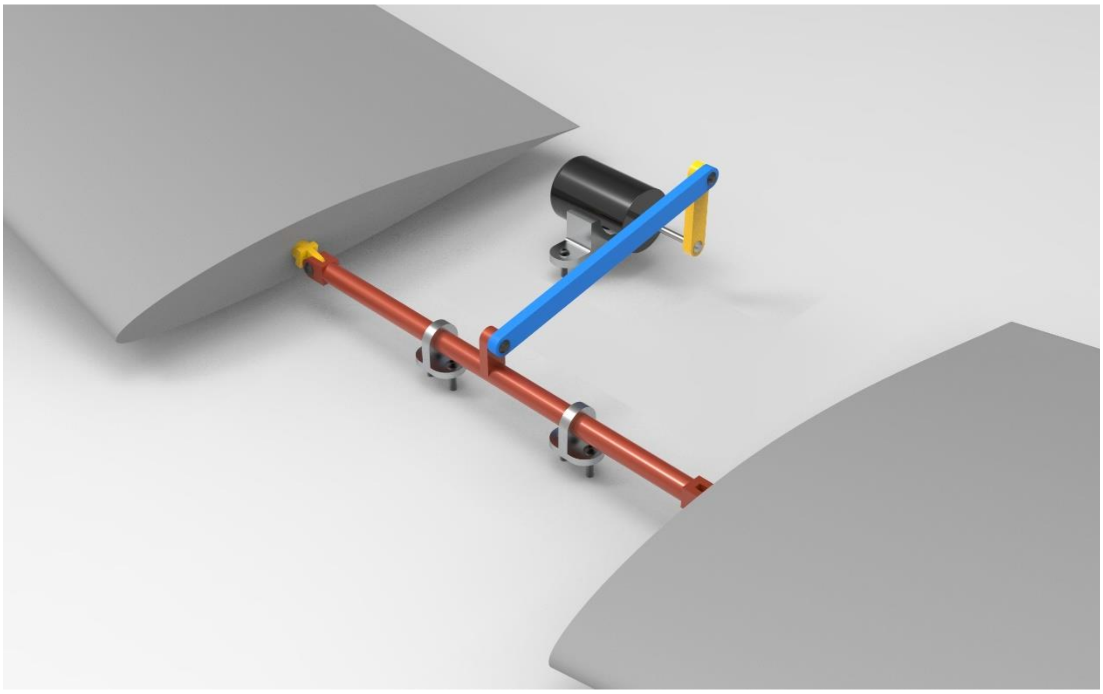

Figure 8.1 Foldable wing mechanism

With the work to be done, an unmanned vehicle that can move both in the air and underwater and consisting of a single design will be designed. In this way, there will be no need to design and manufacture two different unmanned vehicles for different category missions.

While designing air and underwater vehicle in the form of a flying fish, it is planned to protect the electronic systems of the vehicle from the water environment with traditional isolation methods. In the designed system, a foldable wing, which reduces friction by folding underwater and can achieve lift force by opening in air, is designed and shown in Figure 8.1. With the closing of the folding wing in the water, the friction area will be reduced and the speed increase in the water will decrease the power requirement. When the designed air and underwater vehicle enters the water, the folding wing will be closed and the repulsive propeller will be stopped to be ready for operation if necessary.

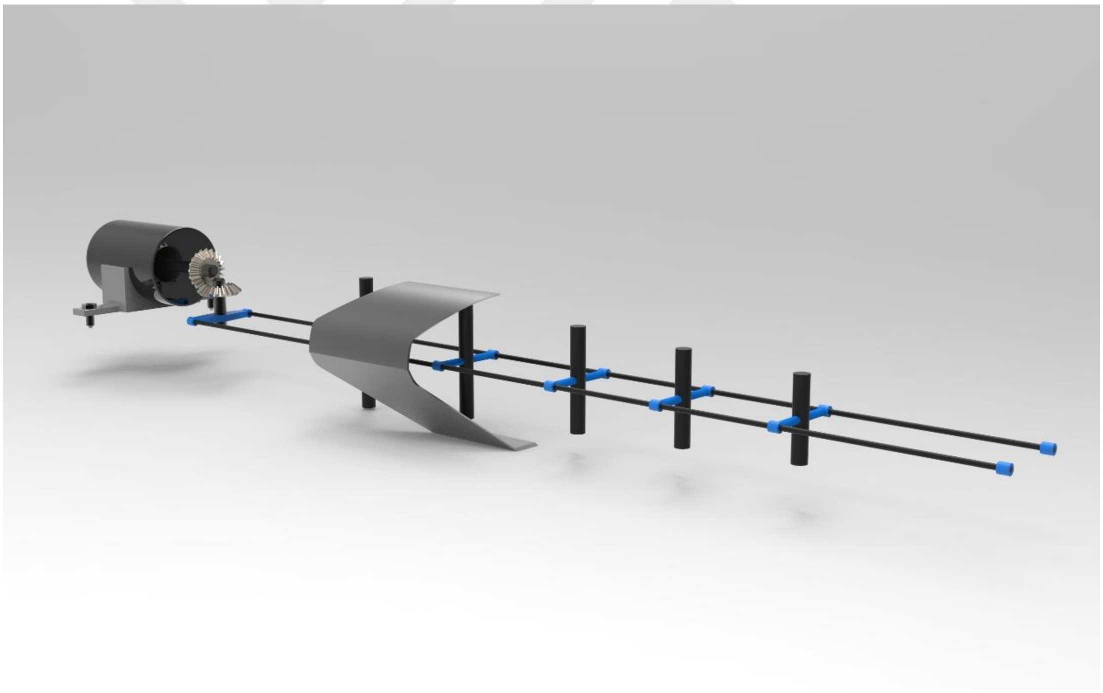

Figure 8.2 Lateral movement tail mechanism

The tail, which can move laterally to ensure its movement and orientation in the water, is designed as shown in Figure 8.2. The tail lateral movement direction is designed to be left and right like in flying fish. In addition, thanks to the flow stabilizers that can be used in both air and water, the vehicle will move stably.

In the designed vehicle, the speed of the movement of the tail mechanism can be increased and the speed of the vehicle in water can be increased, and the propeller will also be useful in increasing the speed of the vehicle in the water. In addition, friction will be minimized in the water thanks to the wings that can be folded in water. The designed system will be able to bring its foldable wings to fixed wing aircraft geometry in the transition to the air environment.

In the method subject to the study, an unmanned vehicle that can move both in the air and underwater with a single design will be designed by changing the unmanned air and underwater vehicle design logic. Since different vehicle design and production will not be made for different category missions with the study, it will provide many benefits economically and ergonomically. Again, in the method subject to the design, it can gain speed thanks to the tail that can move laterally in the water, and it can also be made to direct the vehicle.

REFERENCES

[1] Valavanis, K. P., & Vachtsevanos, G. J. (Eds.). (2015). *Handbook of unmanned aerial vehicles* (Vol. 1). Dordrecht: Springer Netherlands.

[2] Sadraey, M. H. (2012). *Aircraft design: A systems engineering approach*. John Wiley & Sons.

[3] Raymer, D. P. (1992). Aircraft design. *A conceptual approach*.

[4] Turanoğuz, E. (2014). Design of Medium Range Tactical UAV and Improvement of Its Performance by Using Winglets. *Middle East Technical University, Ankara*.

[5] Nicolai, L. M., & Carichner, G. E. (2010). *Fundamentals of aircraft and airship design, Volume 1–Aircraft Design*. American Institute of Aeronautics and Astronautics.

[6] Hassanalian, M., Khaki, H., & Khosravi, M. (2015). A new method for design of fixed wing micro air vehicle. *Proceedings of the Institution of Mechanical Engineers, Part G: Journal of Aerospace Engineering*, *229*(5), 837-850.

[7] Coutinho, W. P., Battarra, M., & Fliege, J. (2018). The unmanned aerial vehicle routing and trajectory optimisation problem, a taxonomic review. *Computers & Industrial Engineering*, *120*, 116-128.

[8] Newcome, L. R. (2004). *Unmanned aviation: a brief history of unmanned aerial vehicles*. American Institute of Aeronautics and Astronautics.

[9] Goh, G. D., Agarwala, S., Goh, G. L., Dikshit, V., Sing, S. L., & Yeong, W. Y. (2017). Additive manufacturing in unmanned aerial vehicles (UAVs): Challenges and potential. *Aerospace Science and Technology*, *63*, 140-151.

[10] Eisenbeiss, H. (2004). A mini unmanned aerial vehicle (UAV): system overview and image acquisition. *International Archives of Photogrammetry. Remote Sensing and Spatial Information Sciences*, *36*(5/W1), 1-7.

[11] Wu, Q., Zeng, Y., & Zhang, R. (2018). Joint trajectory and communication design for multi-UAV enabled wireless networks. *IEEE Transactions on Wireless Communications*, *17*(3), 2109-2121.

[12] Nex, F., & Remondino, F. (2014). UAV for 3D mapping applications: a review. *Applied geomatics*, *6*(1), 1-15.

[13] Hassanalian, M., & Abdelkefi, A. (2017). Classifications, applications, and design challenges of drones: A review. *Progress in Aerospace Sciences*, *91*, 99-131.

[14] Gonçalves, J. A., & Henriques, R. (2015). UAV photogrammetry for topographic monitoring of coastal areas. *ISPRS Journal of Photogrammetry and Remote Sensing*, *104*, 101-111.

[15] Arjomandi, M., Agostino, S., Mammone, M., Nelson, M., & Zhou, T. (2006). Classification of unmanned aerial vehicles. *Report for Mechanical Engineering class, University of Adelaide, Adelaide, Australia*.

[16] Hassanalian, M., Abdelkefi, A., Wei, M., & Ziaei-Rad, S. (2017). A novel methodology for wing sizing of bio-inspired flapping wing micro air vehicles: theory and prototype. *Acta Mechanica*, *228*(3), 1097-1113.

[17] Watts, A. C., Ambrosia, V. G., & Hinkley, E. A. (2012). Unmanned aircraft systems in remote sensing and scientific research: Classification and considerations of use. *Remote Sensing*, *4*(6), 1671-1692.

[18] Dihedral. Available at: https://tr.wikipedia.org/wiki/Dihedral, Accessed 15.10.2020.

[19] Paranjape, A. A., Chung, S. J., & Kim, J. (2013). Novel dihedral-based control of flapping-wing aircraft with application to perching. *IEEE Transactions on Robotics*, *29*(5), 1071-1084.

[20] Goldhammer, M. I., & Schippers, K. A. (1994). *U.S. Patent No. 5,275,358*. Washington, DC: U.S. Patent and Trademark Office.

[21] Platzer, M. F., Jones, K. D., Young, J., & Lai, J. C. (2008). Flapping wing aerodynamics: progress and challenges. *AIAA journal*, *46*(9), 2136-2149.

[22] Triet, N. M., Viet, N. N., & Thang, P. M. (2015). Aerodynamic analysis of aircraft wing. *VNU Journal of Science: Mathematics-Physics, 31*(2).

[23] Chitte, P., Jadhav, P. K., & Bansode, S. S. (2013). Statistic and dynamic analysis of typical wing structure of aircraft using Nastran. *International Journal of Application or Innovation in Engineering & Management*, *2*(7).

[24] Boelens, O. J. (2012). CFD analysis of the flow around the X-31 aircraft at high angle of attack. *Aerospace Science and Technology*, *20*(1), 38-51.

[25] Panagiotou, P., Kaparos, P., & Yakinthos, K. (2014). Winglet design and optimization for a MALE UAV using CFD. *Aerospace Science and Technology*, *39*, 190-205.

[26] Bravo-Mosquera, P. D., Botero-Bolivar, L., Acevedo-Giraldo, D., & Cerón-Muñoz, H. D. (2017). Aerodynamic design analysis of a UAV for superficial research of volcanic environments. *Aerospace Science and Technology*, *70*, 600-614.

[27] Zhao, H., & Bil, C. (2008, August). Aerodynamic design and analysis of a vtol ducted-fan uav. In *26th AIAA Applied Aerodynamics Conference* (p. 7516).

[28] Cao, Y., & Yu, Z. (2005). Numerical simulation of turbulent flow around helicopter ducted tail rotor. *Aerospace Science and Technology*, *9*(4), 300-306.

[29] Davenport, J. (1992). Wing-loading, stability and morphometric relationships in flying fish (Exocoetidae) from the north-eastern Atlantic. *Journal of the Marine Biological Association of the United Kingdom*, *72*(1), 25-39.

[30] Park, H., & Choi, H. (2010). Aerodynamic characteristics of flying fish in gliding flight. *Journal of Experimental Biology*, *213*(19), 3269-3279.

[31] Fish, F. E. (1990). Wing design and scaling of flying fish with regard to flight performance. *Journal of Zoology*, *221*(3), 391-403.

[32] National Geographic, Common Name: Flying Fish, Scientific Name: Exocoetidae. Available at: https://www.nationalgeographic.com/animals/fish/group/flying-fish/, Accessed 08.10.2020.

[33] Alonso, J. J., LeGresley, P., & Pereyra, V. (2009). Aircraft design optimization. *Mathematics and Computers in Simulation*, *79*(6), 1948-1958.

[34] Sobieski, I., & Kroo, I. (1996). Aircraft design using collaborative optimization. In *34th Aerospace Sciences Meeting and Exhibit* (p. 715).

[35] Torenbeek, E. (2013). *Advanced aircraft design: conceptual design, analysis and optimization of subsonic civil airplanes*. John Wiley & Sons.

[36] Hashimoto, A., Jeong, S., & Obayashi, S. (2015). Aerodynamic optimization of near-future high-wing aircraft. *Transactions of the Japan Society for Aeronautical and Space Sciences*, *58*(2), 73-82.

[37] Sarker, M. S., Panday, S., Rasel, M., Salam, M. A., Faisal, K. M., & Farabi, T. H. (2017, December). Detail design of empennage of an unmanned aerial vehicle. In *AIP Conference Proceedings* (Vol. 1919, No. 1, p. 020033). AIP Publishing LLC.

[38] Ciliberti, D., Nicolosi, F., & Della Vecchia, P. (2013, September). A new approach in aircraft vertical tailplane design. In *22th AIDAA Conference*. Associazione Italiana di Aeronautica e Astronautica Naples (Italy).

[39] Divakaran, V. N., Kumar, G. R., & Rao, P. S. (2015). Aircraft landing gear design and development.

[40] Currey, N. S. (1988). *Aircraft landing gear design: principles and practices*. American Institute of Aeronautics and Astronautics.

[41] Baran, D., Tataru, S., & Petre, M. (2018). Preliminary Estimation Methods for the Definition of the Landing Gear. *INCAS Bulletin*, *10*(3), 187-197.

[42] Blondeau, J., Richeson, J., & Pines, D. (2003). Design of a morphing aspect ratio wing using an inflatable telescoping spar. In *44th AIAA/ASME/ASCE/AHS/ASC Structures, Structural Dynamics, and Materials Conference* (p. 1718).

[43] Sadraey, M. (2012). Wing Design. *Aircraft Design: A Systems Engineering Approach*, *808*.

[44] Thomas, J. L., Krist, S. T., & Anderson, W. K. (1990). Navier-Stokes computations of vortical flows over low-aspect-ratio wings. *AIAA journal*, *28*(2), 205-212.

[45] Anderson, J. D. (1999). *Aircraft performance and design*.

[46] Tulapurkara, E. G. (2014). Airplane design (Aerodynamic).

[47] Ciliberti, D., Della Vecchia, P., Nicolosi, F., & De Marco, A. (2017). Aircraft directional stability and vertical tail design: A review of semi-empirical methods. *Progress in Aerospace Sciences*, *95*, 140-172.

[48] Duncan, J. S. (2007). Aircraft Weight and Balance Handbook.

[49] Kontogiannis, S. G., & Ekaterinaris, J. A. (2013). Design, performance evaluation and optimization of a UAV. *Aerospace science and technology*, *29*(1), 339-350.

[50] Rokam, J. (1998). Airplane Flight Dynamics and Automatic Flight Controls (Darcorporation).

[51] Phillips, W. F., & Alley, N. R. (2007). Predicting maximum lift coefficient for twisted wings using lifting-line theory. *Journal of aircraft*, *44*(3), 898-910.

[52] Saarlas, M. (2006). *Aircraft performance*. John Wiley & Sons.

[53] Aircraft Performance. Available at: https://www.faa.gov/regulations_policies/handbooks_manuals/aviation/phak/media/13_phak_ch11.pdf, Accessed 18.11.2020.

[54] Filippone, A. (2012). *Advanced aircraft flight performance* (Vol. 34). Cambridge University Press.

[55] Roskam, J., & Lan, C. T. E. (1997). *Airplane aerodynamics and performance*. DARcorporation.

[56] PBS TP100 Turboprop Engine. Available at: https://www.pbsaerospace.com/our-products/ts-100-turboshaft-engine, Accessed 19.11.2020.

[57] Weierman, J., & Jacob, J. (2010, June). Winglet design and optimization for UAVs. In *28th AIAA Applied Aerodynamics Conference* (p. 4224).

[58] Jamei, S., Maimun, A., Mansor, S., Azwadi, N., & Priyanto, A. (2016). Design Parametric Study of a Compound Wing-in-Ground Effect. II: Aerodynamics Coefficients. Journal of Aerospace Engineering, 29(1), 04015023.

[59] Matsson, J. E. (2013). An Introduction to SolidWorks Flow Simulation 2013. SDC publications.